

# TRIM28 is an essential regulator of three-dimensional chromatin state underpinning CD8<sup>+</sup> T cell activation

Received: 21 January 2024

Accepted: 4 January 2025

Published online: 16 January 2025

 Check for updatesKun Wei<sup>1,6</sup>, Ruifeng Li<sup>1,2,6</sup>, Xiaohong Zhao<sup>1</sup>, Bowen Xie<sup>1,2</sup>, Tian Xie<sup>1</sup>, Qinli Sun<sup>1</sup>, Yongzhen Chen<sup>1</sup>, Peng Wei<sup>1,2</sup>, Wei Xu<sup>1,2</sup>, Xinyi Guo<sup>1,2</sup>, Zixuan Zhao<sup>1</sup>, Han Feng<sup>1</sup>, Ling Ni<sup>1</sup> & Chen Dong<sup>1,3,4,5</sup> ✉

T cell activation is accompanied by extensive changes in epigenome. However, the high-ordered chromatin organization underpinning CD8<sup>+</sup> T cell activation is not fully known. Here, we show extensive changes in the three-dimensional genome during CD8<sup>+</sup> T cell activation, associated with changes in gene transcription. We show that CD8<sup>+</sup> T-cell-specific deletion of *Trim28* in mice disrupts autocrine IL-2 production and leads to impaired CD8<sup>+</sup> T cell activation in vitro and in vivo. Mechanistically, TRIM28 binds to regulatory regions of genes associated with the formation of chromosomal loops during activation. At the loop anchor regions, TRIM28-occupancy overlaps with that of CTCF, a factor known for defining the boundaries of topologically associating domains and for forming of the loop anchors. In the absence of *Trim28*, RNA Pol II and cohesin binding to these regions diminishes, and the chromosomal structure required for the active state is disrupted. These results thus identify a critical role for TRIM28-dependent chromatin topology in gene transcription in activated CD8<sup>+</sup> T cells.

Studies using chromatin conformation capture techniques have revealed that the mammalian genome is organized into high-ordered folding of chromatin in a hierarchy of structures including compartments<sup>1</sup> topologically associating domains (TADs)<sup>2</sup> and chromatin loops<sup>3</sup>. The mammalian genome is organized into gene-dense and transcriptionally active compartment A as well as gene-sparse and transcriptionally inactive compartment B at the mega-base scale<sup>1</sup>. CCCTC-binding factor (CTCF) and cohesin are the master regulators of genome organization<sup>4,5</sup>. Vast studies have proved that CTCF plays a crucial role in the formation of TAD boundaries and loop anchors<sup>2,3</sup>. The majority of TADs are formed by a process called loop extrusion, in which the cohesin complex extrudes chromatin until it is blocked by the CTCF boundaries<sup>6</sup>. More importantly, cohesin deficiency

eliminates all chromatin loops<sup>5</sup>. In the past years, three-dimensional genome (3D genome) has emerged as an important regulator of gene transcription by facilitating or impeding long-range genomic interactions among regulatory elements and gene bodies<sup>7-9</sup>. 3D genome organization have been shown important in cancer<sup>10-12</sup> and embryonic development<sup>13,14</sup>. However, the observation that the high dynamic of 3D genome among different cell types and cell status<sup>3,15,16</sup> has also raised questions that their role in cell- and status-specific regulatory processes. Furthermore, it has remained unclear if alterations in 3D genome can contribute to immune cell activation and differentiation.

CD8<sup>+</sup> T cells play a major role in adaptive immune response by destroying infected cells and tumor cells. Naive CD8<sup>+</sup> T cells are activated by their cognate antigens on antigen-presenting cells. Naive

<sup>1</sup>Institute for Immunology, Tsinghua University, Beijing 100084, China. <sup>2</sup>Peking University-Tsinghua University Joint Center for Life Sciences, Tsinghua University, Beijing 100084, China. <sup>3</sup>Shanghai Immune Therapy Institute, Shanghai Jiao Tong University School of Medicine-Affiliated Renji Hospital, Shanghai 200127, China. <sup>4</sup>Research Unit of Immune Regulation and Immune Diseases of Chinese Academy of Medical Sciences, Shanghai Jiao Tong University School of Medicine-Affiliated Renji Hospital, Shanghai 200127, China. <sup>5</sup>Westlake University School of Medicine, Hangzhou, Zhejiang 310030, China. <sup>6</sup>These authors contributed equally: Kun Wei, Ruifeng Li. ✉e-mail: [dongchen@westlake.edu.cn](mailto:dongchen@westlake.edu.cn)

CD8<sup>+</sup> T cells undergo rapid clonal expansion and develop into effector cytotoxic T cells, as a result of signaling from T cell receptor (TCR), co-stimulatory molecules, and cytokines<sup>17</sup>. Numerous studies have shown that autocrine IL-2 signals promote CD8<sup>+</sup> T cell activation. Activated CD8<sup>+</sup> T cells, distinct from naive and memory CD8<sup>+</sup> T cells, highly express activation markers CD25, CD44, CD69, ICOS, etc., and produce effector molecules, such as Granzyme B and IFN- $\gamma$ , which exert anti-microbial and anti-tumor functions<sup>18</sup>. Epigenetic mechanisms have been reported to be key in T cell activation<sup>19</sup>. Compared with naive CD8<sup>+</sup> T cells, activated CD8<sup>+</sup> T cells harbor different DNA and histone modifications, including increased permissive histone markers H3K4me3 and H3K27ac at loci of activation-induced genes, such as transcription factors *Tbx21*, *Id2*, *Batf* and *Nfat1* as well as effector-associated genes, including *Il2ra*, *Ifng*, *Il2* and *Icos*<sup>20</sup>. Naive and activated CD8<sup>+</sup> T cells also show distinct chromatin accessibility features<sup>21</sup>. However, whether and how 3D genome reorganizes during CD8<sup>+</sup> T cell activation are unclear.

Tripartite motif (TRIM)-containing proteins are defined by the presence of an N-terminal RING finger, one or two B-boxes and a coiled-coil (CC) domain<sup>22</sup>. They function in a wide range of cellular processes including cell differentiation, antiviral activity, autophagy and immune response<sup>23</sup>. Recent studies have shown that many TRIM proteins serve as critical regulators of innate and adaptive immunity: TRIM33 promotes the pro-inflammatory function of Th17 cells<sup>24</sup>; TRIM28 regulates Th17 and Treg function<sup>25,26</sup> and TRIM5 restricts HIV-1 infection<sup>27</sup>. Though not directly binding to DNA, TRIM proteins can regulate gene expression as co-regulators by interacting with chromatin modifiers<sup>28–30</sup>. Among them, TRIM33 can act as a mediator in remodeling chromatin at distal regulatory elements and in transcription regulation<sup>31</sup>. TRIM28 was previously reported as a transcriptional elongation factor to regulate gene expression<sup>32</sup>. However, the function of TRIM proteins in CD8<sup>+</sup> T cell activation remained unknown.

In this study, we systematically characterize the 3D genome reorganization at compartment, TAD and loop levels during CD8<sup>+</sup> T cell activation. TRIM28 is required for the transcriptional program in activated CD8<sup>+</sup> T cells, whose deficiency impaired their effector function in tumor and infection. Mechanistically, TRIM28 regulates the expression of target genes by cooperating with CTCF, RNA Pol II and cohesin to mediate the formation of chromatin loops. Altogether, this study unveils TRIM28-dependent 3D genome re-organization as an essential epigenetic mechanism underlying CD8<sup>+</sup> T cell activation.

## Results

### CD8<sup>+</sup> T cell activation is accompanied by extensive spatial chromatin changes

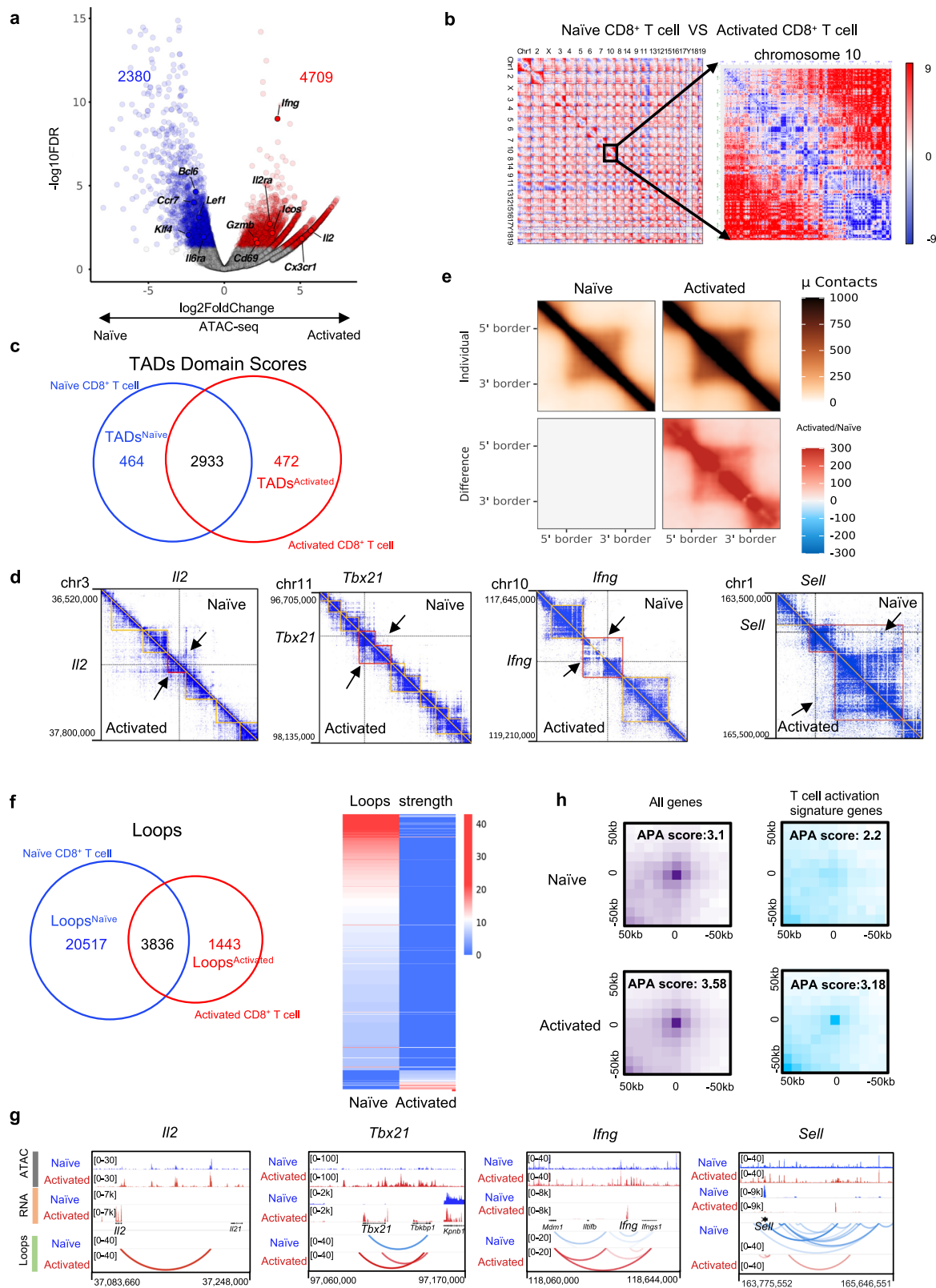
To identify the chromatin changes during CD8<sup>+</sup> T cell activation, we sorted naive CD8<sup>+</sup> T cells from C57BL/6 mice and treated them with anti-CD3 and anti-CD28 for 3 days in vitro. Then, we did Assay for Transposase-Accessible Chromatin with high-throughput sequencing (ATAC-seq) and high-through chromosome conformation capture (Hi-C) experiments on activated and naive CD8<sup>+</sup> T cells (Supplementary Fig. 1a, b). We found that activated CD8<sup>+</sup> T cells were distinct from naive CD8<sup>+</sup> T cells in the epigenome based on the ATAC-seq data (Fig. 1a). We examined 45,876 chromatin accessible regions in these two types of T cells and searched for differentially accessible regions (Fig. 1a). Overall, 4709 (10%) chromatin regions were more accessible in activated CD8<sup>+</sup> T cells, whereas 2380 (5.2%) chromatin regions less accessible, than in naive CD8<sup>+</sup> T cells (Fig. 1a). T cell activation signature genes, such as *Il2*, *Ifng*, *Tbx21* and *Gzmb* showed increased accessibility in activated CD8<sup>+</sup> T cells whereas naive T cell signature genes, such as *Ccr7*, *Slamf6* and *Lef1* showed decreased accessibility after T cell activation (Fig. 1a, Supplementary Fig. 1c). Binding of T cell activation-related transcription factors, such as Fos, JunB and BATF was predicted to be increased in genome of activated CD8<sup>+</sup> T cells, compared with naive CD8<sup>+</sup> T cells (Supplementary Fig. 1d). These

results demonstrated significant alterations in chromatin accessibility during CD8<sup>+</sup> T cell activation.

For naive and activated CD8<sup>+</sup> T cells, we constructed two Hi-C libraries for each sample. For each Hi-C library, about 250 million unique mapped contacts were generated (Supplementary Table 1). The replicates were highly correlated (Supplementary Fig. 1b, SCC score  $R \geq 0.95$ )<sup>33</sup> and we therefore merged the data for visualization purposes. The contact quality of the Hi-C data was validated by cis/trans interaction ratio (Supplementary Table 1). We reached a fine resolution of 5 kilobase pairs (kb) which enabled us to explore 3D genome structure at different scales, such as A/B compartments, TADs and loop structures of all the samples. Across the whole genome, naive CD8<sup>+</sup> T cells had more long-range interactions (> 10 Mb), whereas activated CD8<sup>+</sup> T cells had more short-range interactions (<100 kb) (Fig. 1b, Supplementary Fig. 1e). In naive CD8<sup>+</sup> T cells, 49% genomic regions were identified as compartment A, and 51% genomic regions were identified as compartment B. Most genomic regions (93%) remained in the same compartments in activated CD8<sup>+</sup> T cells compared with naive CD8<sup>+</sup> T cells (Supplementary Fig. 1f). A total of 4.6% of genomic regions switched from compartment A to B after activation of CD8<sup>+</sup> T cells, whereas 2.3% of genomic regions did the opposite switch (Supplementary Fig. 1f). In terms of interactions between compartments, activated CD8<sup>+</sup> T cells had less intra compartment interaction (Supplementary Fig. 1g).

Separately examining the matrices of activated and naive CD8<sup>+</sup> T cells, we identified 2191 TADs in naive CD8<sup>+</sup> T cells and 2501 TADs in activated CD8<sup>+</sup> T cells. Most (80%) of the boundaries of TADs were unchanged during CD8<sup>+</sup> T cell activation. The domain score was a measure for the degree of connectivity within a TAD<sup>16</sup>. For each TAD, we calculated the domain score as the fraction of intradomain contacts over its total numbers of cis contacts. In activated CD8<sup>+</sup> T cells, 464 TADs had decreased domain scores which were defined as TADs<sup>naive</sup> and 472 TADs had increased domain scores which were defined as TADs<sup>activated</sup> (Fig. 1c, Supplementary Fig. 1h). 1717 genes located in TADs<sup>naive</sup> included many naive T cell signature genes, such as *Sell*, *Ccr7* and *Tcf7*, whose expression showed a clear downregulation after T cell activation (Fig. 1d, Supplementary Fig. 1i). On the contrary, 2548 genes located in TADs<sup>activated</sup> were enriched in those associated with T cell activation, such as *Il2*, *Tbx21* and *Ifng*, whose expression showed a clear upregulation in activated T cells (Fig. 1d, Supplementary Fig. 1i). In naive CD8<sup>+</sup> T cells, *Il2* was located in a TAD with 286-kb in length. The domain score of this TAD was increased by 30% in activated CD8<sup>+</sup> T cells (Fig. 1d). Similarly, the domain scores of the TADs where *Tbx21* and *Ifng* are located were increased after T cell activation. Specially, the TAD where *Tbx21* is located (484 kb) merged with the downstream TAD into one TAD (Fig. 1d). On the contrary, the domain score of the TAD where *Sell* is located was decreased after T cell activation (Fig. 1d). To further investigate the alterations in the 3D genome at CD8<sup>+</sup> T cell activation-related genes, 358 genes with upregulated expression (Fold change ( $\log_2$ ) > 1,  $q$ -value < 0.01) were identified during CD8<sup>+</sup> T cell activation using the public RNA-seq data<sup>34</sup>. The domain scores of the TADs where these genes are located were calculated, which were found to be increased in activated compared to naive CD8<sup>+</sup> T cells (Fig. 1e).

Within TADs, chromatin loops facilitate long-range interactions between enhancers and promoters for gene regulation<sup>3</sup>. There were 1443 unique loops in activated CD8<sup>+</sup> T cells, which were defined as Loops<sup>activated</sup>, and 20,517 ones in naive CD8<sup>+</sup> T cells, defined as Loops<sup>naive</sup>, with 3836 in both lists (Fig. 1f). Loops<sup>naive</sup> and Loops<sup>activated</sup> were validated using APA plots (Supplementary Fig. 1j). 3254 genes were located in naive CD8<sup>+</sup> T cell-specific loops, such as *Sell*, *Ccr7* and *Tcf7* (Fig. 1g). 2316 genes were located in activated CD8<sup>+</sup> T cell-specific loops, such as *Il2*, *Tbx21* and *Ifng*. The genes located in the anchor regions of Loops<sup>naive</sup> were enriched in mRNA processing genes, whereas those in Loops<sup>activated</sup> were associated with T cell activation



genes (Supplementary Fig. 1k). Among the genes located on the dynamically regulated chromosomal loops during CD8<sup>+</sup> T cell activation, 2228 genes were differentially expressed between naive and activated WT CD8<sup>+</sup> T cells and enriched in regulation of T cell activation and mononuclear cell differentiation pathways. 3342 genes were not differentially expressed between the two cells, enriched in mRNA processing and ribonucleoprotein complex biogenesis. In naive CD8<sup>+</sup>

T cells, there was no loop around *I12*. However, a significant loop was formed between *I12* promoter and an upstream chromatin accessible region during CD8<sup>+</sup> T cell activation (Fig. 1g). Similarly, the loop strengths for *Tbx21* and *Ifng* were increased after T cell activation (Fig. 1g). On the contrary, most of loops where *Sell* is located disappeared in activated CD8<sup>+</sup> T cells (Fig. 1g). Then, the strengths of the loops where 358 T cell activation genes are located were calculated. We

**Fig. 1 | The activation-associated genes are involved in the chromatin spatial structures in CD8<sup>+</sup> T cells.** **a** Volcano plot of chromatin accessibility data in activated versus naive CD8<sup>+</sup> T cells. Red dots represented chromatin regions which were more accessible in activated CD8<sup>+</sup> T cells (Fold change ( $\log_2$ ) > 0.58, p-value < 0.05). Blue dots represented chromatin regions which were more accessible in naive CD8<sup>+</sup> T cells (Fold change ( $\log_2$ ) < -0.58, p-value < 0.05). Every sample has two replicates. **b** The heatmap of per-bin Fold change ( $\log_2$ ) in Hi-C interactions of activated and naive CD8<sup>+</sup> T cells of the whole genome (left) and chromosome 10 (right). Red represents stronger interaction in naive CD8<sup>+</sup> T cells, blue means stronger interaction in activated CD8<sup>+</sup> T cells. Every sample has two replicates. **c** Venn diagram of the TADs of activated and naive CD8<sup>+</sup> T cells based on domain scores. TADs, topologically associating domains. Two replicates were analyzed separately to assess consistency, and results were then combined. Details see

methods. **d** Hi-C interaction matrix of the regions in naive and activated CD8<sup>+</sup> cells around the *Il2*, *Tbx21* *Ifng* and *Sell* genes. **e** ATA plot showing the TADs where T cell activation-related genes were located in naive and activated CD8<sup>+</sup> T cells. ATA, aggregate TAD analyses. **f** Venn diagram of the chromatin loops of activated and naive CD8<sup>+</sup> T cells (left). Heatmap of loop strength ( $-\log_{10}$ fdrBL) difference (right). Two replicates were analyzed separately to assess consistency, and the results were then combined. For details see methods. **g** Genome browser view of chromatin accessibility, gene expression, and 3D genome interactions around the *Il2* *Tbx21* *Ifng* and *Sell* genes in naive and activated CD8<sup>+</sup> T cells. **h** APA plot for the loops where T cell activation genes were located in naive and activated CD8<sup>+</sup> T cells. APA, aggregate peak analysis. Statistical significance was tested by unpaired two-tailed Student's t test (**h**).

found the average strengths of these loops were increased after T cell activation, which implicates regulation of T cell activation genes by the 3D chromatin structure (Fig. 1h, Supplementary Fig. 1l).

These results indicated that CD8<sup>+</sup> T cells activation is accompanied by extensive changes in the chromatin accessibility and 3D genome. Importantly, the alteration in high-ordered chromosomal structure was closely related to the regulation of T cell activation-related genes.

### TRIM28 is required for CD8<sup>+</sup> T cell activation and function

TRIM proteins have been reported to regulate gene expression as coregulators in immune cells<sup>28–30</sup>. However, their roles during CD8<sup>+</sup> T cell activation remained unknown. We expect that TRIM proteins may regulate CD8<sup>+</sup> T cell activation through epigenetic mechanisms. So, we first analyzed public RNA-seq data of mouse naive and activated CD8<sup>+</sup> T cells to explore expression changes of TRIM family members during CD8<sup>+</sup> T cell activation<sup>34</sup>. Some TRIM family members like *Trim28*, *Trim27*, *Trim37* and *Trim16* expression was found to be substantially elevated in activated CD8<sup>+</sup> T cells, as compared to naive CD8<sup>+</sup> T cells (Fig. 2a). Interestingly, *Trim28* expression was found to be highest as compared to other TRIM family members in activated CD8<sup>+</sup> T cells (Supplementary Fig. 2a). Moreover, ATAC-seq data indicated the chromatin accessibility of *Trim28* was increased in activated CD8<sup>+</sup> T cells (Supplementary Fig. 2b). Meanwhile, a significant loop was formed around the *Trim28* locus during CD8<sup>+</sup> T cell activation (Supplementary Fig. 2b). To confirm these results, we measured mRNA levels of *Trim28* and found that it was highly expressed in activated, as compared to naive CD8<sup>+</sup> T cells in mice (Fig. 2b).

To investigate the function of TRIM28 during CD8<sup>+</sup> T cell activation, we generated *Trim28<sup>fl/fl</sup>Cd8a<sup>Cre</sup>* mice, in which *Trim28* was specifically deleted in mature CD8<sup>+</sup> T cells (hereafter as *Trim28<sup>-/-</sup>* mice). Although it was previously reported that *Trim28* deficiency in T cells resulted in reduced numbers of T cells in the peripheral<sup>35</sup>, peripheral CD8<sup>+</sup> T cell-specific deletion of *Trim28* had no apparent effect on the development of T cells in both thymus and peripheral (Supplementary Fig. 2c). We then evaluated the impact of *Trim28* deficiency on CD8<sup>+</sup> T cell activation. Naive CD8<sup>+</sup> T cells were isolated from *Trim28<sup>fl/fl</sup>* and *Trim28<sup>-/-</sup>* mice and activated with anti-CD3 plus anti-CD28 for 3 days in vitro. *Trim28* ablation led to reduced IFN- $\gamma$ , TNF- $\alpha$  and Granzyme B expression after CD8<sup>+</sup> T cell activation (Fig. 2c, Supplementary Fig. 2e), which indicated that *Trim28* deficiency impaired effector differentiation of CD8<sup>+</sup> T cells. Transcription factor T-bet is critical in controlling the expression of genes encoding effector molecules in activated CD8<sup>+</sup> T cells<sup>36</sup>. Notably, T-bet expression was decreased in activated *Trim28<sup>-/-</sup>* CD8<sup>+</sup> T cells, compared with wild-type controls (Fig. 2d). Further studies showed that loss of *Trim28* also reduced mRNA levels of the *Ifng*, *Gzmb*, *Trnfa*, *Il2*, *Il2ra* and *Tbx21* genes (Fig. 2e).

To globally analyze the genes regulated by TRIM28, we performed RNA-seq analysis of *Trim28<sup>fl/fl</sup>* vs *Trim28<sup>-/-</sup>* CD8<sup>+</sup> T cells activated in vitro as above (Supplementary Fig. 2f). Expression of 1190 genes was reduced, while that of 1412 genes elevated by the deficiency of *Trim28*

(Fig. 2f). Via GO pathway analysis, we characterized the immunological programs regulated by TRIM28. The top listed pathways of the downregulated genes included T cell activation, positive regulation of cytokine production and cytokine-mediated signaling pathway. Meanwhile, the top listed pathways of upregulated genes in *Trim28*-deficient T cells were DNA replication, DNA repair and catalytic activity pathways (Fig. 2g). Specifically, the mRNA expression of numerous T cell activation-related surface molecules (*Icos*, *Entpd1*, *Cx3cr1* and etc.), cytotoxicity molecules (*Ifng*, *Gzmb*, *Il2*, *Gzmk* and etc.) and transcriptional factors (*Tbx21*, *Prdm1*, *Id2* and etc.) were significantly downregulated, while the expression of naive CD8<sup>+</sup> T cell-associated surface molecules (*Ccr7*, *Slamf6*, *Btla* and etc.) and transcriptional factors (*Id3*, *Tcf7* and etc.) were increased in activated *Trim28<sup>-/-</sup>* than control CD8<sup>+</sup> T cells (Fig. 2h). The expression of T cell activation markers like CD25, ICOS and CD69 were decreased in activated *Trim28<sup>-/-</sup>* CD8<sup>+</sup> T cells at the protein level (Supplementary Fig. 2g-i). Consistent with the above flow cytometric results, GSEA analyses revealed that activated *Trim28<sup>-/-</sup>* CD8<sup>+</sup> T cells were more transcriptionally related to naive CD8<sup>+</sup> T cells (Fig. 2i). *Trim28* ablation also dramatically inhibited the proliferation of activated CD8<sup>+</sup> T cells in vitro (Supplementary Fig. 2j). Meanwhile, the percentages of apoptotic cells in *Trim28<sup>-/-</sup>* CD8<sup>+</sup> T cells were significantly increased (Supplementary Fig. 2k), resulting in reduced numbers of live CD8<sup>+</sup> T cells, as compared to activated WT CD8<sup>+</sup> T cells (Supplementary Fig. 2l). Taken together, these results indicated TRIM28 is a crucial positive regulator of CD8<sup>+</sup> T cell activation in vitro.

Naive CD8<sup>+</sup> T cells activated in draining lymph node migrate to tumors and infected organs to exert effector functions<sup>37</sup>. To further identify the roles of TRIM28 in regulating the functions of CD8<sup>+</sup> T cells in vivo, we inoculated *Trim28<sup>fl/fl</sup>Cd8a<sup>Cre</sup>* mice and *Trim28<sup>fl/fl</sup>* mice with E.G7 tumor cells. *Trim28* deficiency resulted in enhanced growth of E.G7 tumors (Fig. 3a, Supplementary Fig. 3a). As a result of *Trim28* deficiency, the frequencies and numbers of CD8<sup>+</sup> T cells were decreased in tumors (Supplementary Fig. 3b). More importantly, the frequencies of antigen-specific CD8<sup>+</sup> TILs were significantly reduced in E.G7-bearing *Trim28<sup>-/-</sup>* mice (Fig. 3b). In addition, the cytotoxic function of *Trim28<sup>-/-</sup>* CD8<sup>+</sup> TILs, compared with wild-type counterparts, was dramatically reduced as indicated by decreased expression of IFN- $\gamma$  (Fig. 3c), Granzyme B (Fig. 3d) and TNF- $\alpha$  (Supplementary Fig. 3c) in E.G7 tumor model. Previous studies found that transcription factors T-bet<sup>38</sup> and TOX<sup>39</sup> regulate CD8<sup>+</sup> T cell function in tumors. *Trim28* deficiency also inhibited the expression of T-bet (Fig. 3e) and TOX (Supplementary Fig. 3d) in CD8<sup>+</sup> TILs. In the tumor-draining lymph nodes (TDLNs), IFN- $\gamma$  production was also significantly defective in *Trim28<sup>-/-</sup>* CD8<sup>+</sup> T cells (Supplementary Fig. 3e).

To further confirm the roles of TRIM28 in antigen-specific CD8<sup>+</sup> T cell activation in vivo, we crossed *Trim28<sup>fl/fl</sup>Cd8a<sup>Cre</sup>* mice with OT-I strain, and transfer equal numbers of naive OT-I cells from these and control *Trim28<sup>fl/fl</sup>* OT-I mice into CD45.1 recipients inoculated with E.G7 tumors. Consistent with above results, enhanced growth of E.G7 tumors was observed in mice receiving *Trim28*-deficient OT-I cells (Fig. 3f). CD45.2 OT-I TIL frequencies among CD8<sup>+</sup> TILs from E.G7

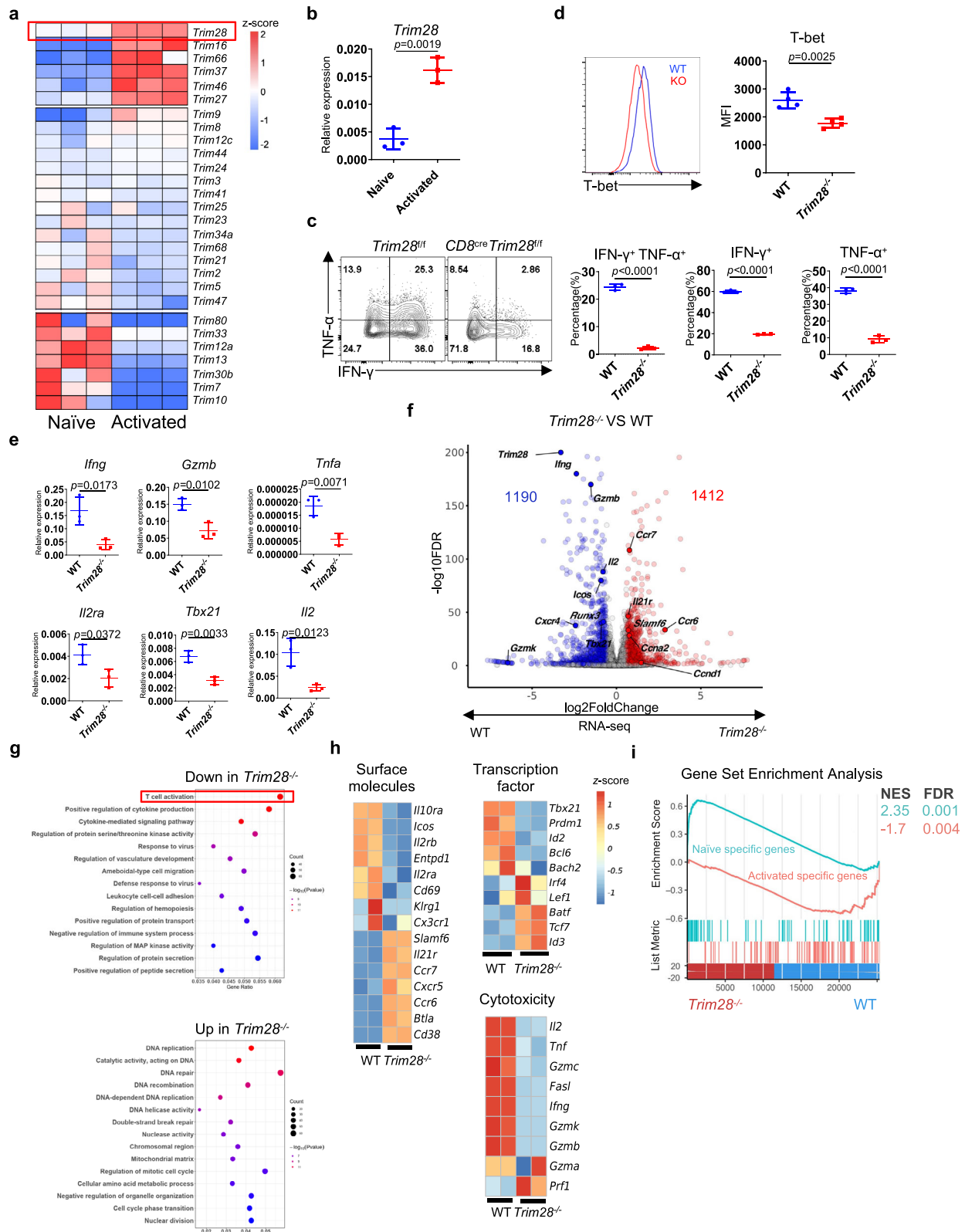


**Fig. 2 | *Trim28* deficiency impairs CD8<sup>+</sup> T cell activation in vitro.** **a** Gene-expression heatmap for the RNA-seq data of TRIM family in murine naive and activated CD8<sup>+</sup> T cells. **b–e** naive CD8<sup>+</sup> T cells were cultured under anti-CD3/28 stimulation for 3 days. Expression of *Trim28* was measured by qPCR (**b**). Expression of IFN- $\gamma$ , TNF- $\alpha$  (**c**) and T-bet (**d**) was measured by flow cytometry. mRNA levels of *Ifng*, *Gzmb*, *Tnfa*, *Il2ra*, *Il2* and *Tbx21* were detected by qPCR (**e**). **f** Volcano plot of transcriptome differences between WT and *Trim28<sup>-/-</sup>* activated CD8<sup>+</sup> T cells. **g** Top

enriched GO pathways of genes regulated by TRIM28. **h** Heatmap of illustrating the relative expression of signature genes in WT and *Trim28<sup>-/-</sup>* activated CD8<sup>+</sup> T cells. **i** GSEA enrichment of naive and activated CD8<sup>+</sup> T cell signature genes in the transcriptome of CD8<sup>+</sup> T cells from *Trim28<sup>fl/fl</sup>CD8a<sup>Cre</sup>* mice. Each dot represents one individual replicate ( $n=3$  per group in **b**, **c** and **e**,  $n=4$  per group in (**d**). Error bars represent the SD. Statistical significance was tested by unpaired two-sided Student's *t*-test (**b–e**). Data are representative of three independent experiments.

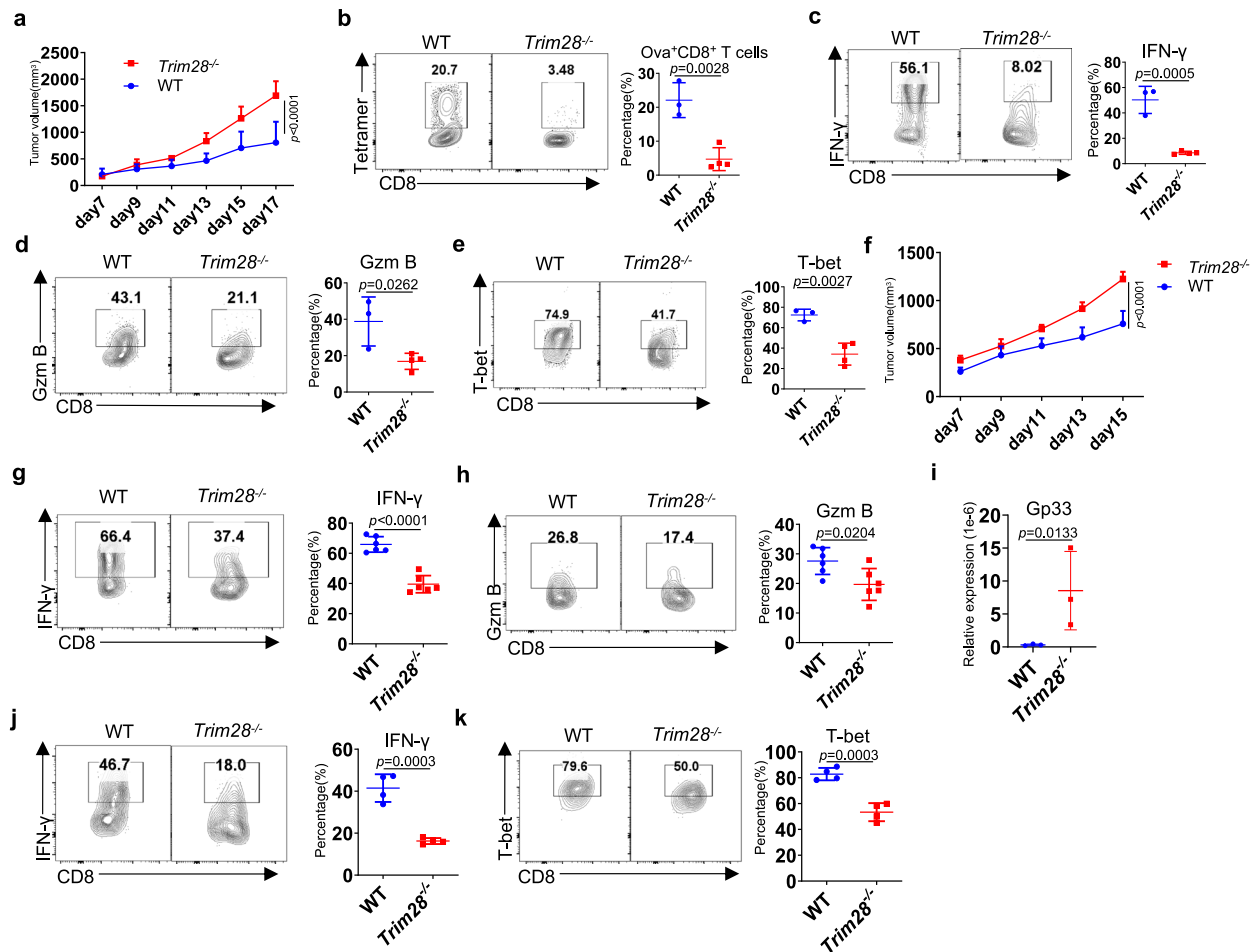


**Fig. 3 | CD8-specific deletion of TRIM28 results in defective function of CD8<sup>+</sup> T cells in tumor and infection.** **a–e** *Trim28*<sup>fl/fl</sup>Cd8a<sup>Cre</sup> mice and control mice were inoculated with E.G7 tumor cells. Mice were ethically euthanized using carbon dioxide asphyxiation and analyzed at day 17 post inoculation. Mean tumor volume of intradermal E.G7 implants in WT versus *Trim28*<sup>-/-</sup> mice (**a**). H-2K(b) tetramer<sup>+</sup> CD8<sup>+</sup> T cells among total CD8<sup>+</sup> T cells (**b**). Flow cytometry analysis showing IFN- $\gamma$  (**c**), Granzyme B (**d**) and T-bet (**e**) expression in CD8<sup>+</sup> TILs. **f–h** naive *Trim28*<sup>-/-</sup> and WT OT-I cells were sorted, and 1 million cells were i.v. transferred into CD45.1 mice. Recipient mice were inoculated with  $1 \times 10^6$  EG7 tumor cells at day 1 post transfer. Mice were ethically euthanized using carbon dioxide asphyxiation and analyzed at day 15 post inoculation. Mean tumor volume of intradermal E.G7 implants in WT

OT-I versus *Trim28*<sup>-/-</sup> OT-I group (**f**). Expression of IFN- $\gamma$  (**g**) and Granzyme B (**h**) in CD8<sup>+</sup> TILs. **i–k** *Trim28*<sup>-/-</sup> and WT mice were infected i.v. with LCMV Armstrong ( $2 \times 10^5$  pfu), and spleens were collected and analyzed at day 8 post infection. i.v., intravenous injection. **i** Viral loads were measured by qPCR. **j** Expression of IFN- $\gamma$  by antigen-specific CD8<sup>+</sup> T cells was measured. **k** Representative FACS plots showing T-bet expression in antigen-specific CD8<sup>+</sup> T cells. Each dot represents one individual mouse ( $n = 4$  per group in **a–e**, **j–k**,  $n = 6$  per group in **f–h**). Error bars represent the SD. Statistical significance was tested by two-way ANOVA (**a**, **f**) and unpaired two-sided Student's *t*-test (**b–e**, **g–k**). Data are representative of two (**i–k**) and three (**a–h**) independent experiments.

tumors were significantly decreased after *Trim28* deficiency (Supplementary Fig. 3f). Importantly, the cytotoxic function of *Trim28*<sup>-/-</sup> OT-I cells was dramatically reduced in tumors (Fig. 3g, h). These results demonstrated that TRIM28 plays a critical role in anti-tumor function of CD8<sup>+</sup> T cells.

To also analyze *Trim28*-deficient T cells in a competitive setting, we co-transferred equal numbers of naive CD45.2 *Trim28*<sup>-/-</sup> OT-I cells and CD45.1/2 *Trim28*<sup>fl/fl</sup> OT-I cells into E.G7 tumor-bearing CD45.1 recipients. The frequencies of *Trim28*<sup>-/-</sup> OT-I cells among total CD8<sup>+</sup> TILs were dramatically reduced as compared to *Trim28*<sup>fl/fl</sup> OT-I cells on day 15 post inoculation (Supplementary Fig. 3g). Consistent with above results, *Trim28* deficiency resulted in impaired function of activated CD8<sup>+</sup> T cells (Supplementary Fig. 3h, i). These results indicated that TRIM28 was intrinsically required for the cytotoxic function of antigen-specific CD8<sup>+</sup> T cells in the context of cancer.

Activated CD8<sup>+</sup> T cells are also important in clearance of viral infection besides anti-tumor function. Thus, control *Trim28*<sup>fl/fl</sup> and *Trim28*<sup>fl/fl</sup>Cd8a<sup>Cre</sup> mice were infected with LCMV Armstrong virus. Firstly, virus clearance was reduced as a result of *Trim28* deficiency

(Fig. 3i). At day 8 post infection, the total numbers of CD8<sup>+</sup> T cells were dramatically decreased in the infected spleens in the absence of *Trim28*, so did the antigen-specific activated CD8<sup>+</sup> T cells (Supplementary Fig. 3j). Examining surface molecules related with T cell activation, the expression of CD44, CX3CR1 and KLRG1 was decreased in gp33-specific CD8<sup>+</sup> T cells (Supplementary Fig. 3k). Meanwhile, the cytotoxic function of CD44<sup>+</sup> gp33-specific *Trim28*<sup>-/-</sup> CD8<sup>+</sup> T cells were dramatically reduced as indicated by decreased production of IFN- $\gamma$  (Fig. 3j) and Granzyme B (Supplementary Fig. 3k). Moreover, T-bet expression in CD44<sup>+</sup> gp33-specific *Trim28*<sup>-/-</sup> CD8<sup>+</sup> T cells was significantly lower than in control CD8<sup>+</sup> T cells (Fig. 3k).

Overall, these results indicated that *Trim28* deficiency impaired the effector function of CD8<sup>+</sup> T cells in both infection and tumor models.

### TRIM28 regulates IL-2 production to promote CD8<sup>+</sup> T cell activation

From above results, TRIM28 appears to have crucial roles during CD8<sup>+</sup> T cell activation. We therefore investigated the underlying

mechanisms. The top listed pathways of the downregulated genes in *Trim28*<sup>-/-</sup> activated CD8<sup>+</sup> T cells included positive regulation of cytokine production and cytokine-mediated signaling pathway. Multiple cytokines have been implicated in promoting CD8<sup>+</sup> T cell activation like IL-2, IL-12, IL-15 and etc.<sup>40</sup>. However, since there were only CD8<sup>+</sup> T cells in our culture system, we speculated TRIM28 may promote CD8<sup>+</sup> T cell activation through regulating IL-2 production. Thus, to test this hypothesis, we first analyzed IL-2 cytokine production in the absence of *Trim28*. The expression of IL-2 was significantly decreased in activated *Trim28*<sup>-/-</sup> CD8<sup>+</sup> T cells, compared with WT cells (Fig. 4a). Then, to test if IL-2 deficiency played a critical role in *Trim28*<sup>-/-</sup> CD8<sup>+</sup> T cells, we cultured WT and *Trim28*<sup>-/-</sup> naive CD8<sup>+</sup> T cells with or without IL-2 during stimulation with anti-CD3 and anti-CD28 for 3 days in vitro. *Trim28*<sup>-/-</sup> activated CD8<sup>+</sup> T cells cultured with IL-2 expressed comparable cytotoxic molecules as WT CD8<sup>+</sup> T cells without IL-2; adding IL-2 rescued the expression of IFN- $\gamma$  (Fig. 4b), Granzyme B (Supplementary Fig. 4a) and TNF- $\alpha$  (Supplementary Fig. 4b) in *Trim28*<sup>-/-</sup> CD8<sup>+</sup> T cells. *Trim28*<sup>-/-</sup> CD8<sup>+</sup> T cells cultured with IL-2 expressed comparable levels of T-bet and CD25 (Supplementary Fig. 4b) molecules compared with WT CD8<sup>+</sup> T cells without IL-2. Consistent with the above flow cytometric results, qPCR analysis indicated that IL-2 treatment could rescue the phenotypes of *Trim28* deficiency (Supplementary Fig. 4c). To investigate whether a reduction in IL-2 expression occurred in TRIM28-deficient CD8<sup>+</sup> T cells in vivo, we infected *Trim28*<sup>fl/fl</sup>/*Cd8a*<sup>Cre</sup> mice and their littermate *Trim28*<sup>fl/fl</sup> mice with LCMV Armstrong virus. The percentages of IL-2-producing gp33-specific CD8<sup>+</sup> T cells in spleens were significantly decreased by *Trim28* deletion (Fig. 4c). Next, we tested whether administration of IL-2 could rescue phenotypes of *Trim28* deficiency in vivo. *Trim28*<sup>fl/fl</sup>/*Cd8a*<sup>Cre</sup> mice and their littermate *Trim28*<sup>fl/fl</sup> mice were infected with LCMV Armstrong virus. Then, they were intraperitoneally injected with or without mIL-2 (10  $\mu$ g per mouse) every two days starting from day 1. *Trim28*<sup>-/-</sup> CD8<sup>+</sup> T cells in IL-2 treatment group expressed comparable CD44 (Supplementary Fig. 4d) and ICOS (Supplementary Fig. 4e) as WT CD8<sup>+</sup> T cells without IL-2 treatment. Administration of IL-2 rescued the expression of IFN- $\gamma$  in *Trim28*<sup>-/-</sup> gp33-specific CD8<sup>+</sup> T cells (Fig. 4d). These results indicated that administration of IL-2 could rescue the defects of *Trim28*<sup>-/-</sup> CD8<sup>+</sup> T cells in LCMV Armstrong infection.

To further confirm that *Trim28* deficiency impaired CD8<sup>+</sup> T cell activation through downregulating IL-2 production, we isolated naive CD8<sup>+</sup> T cells from WT and *Trim28*<sup>-/-</sup> mice and conducted T-cell activation with or without anti-IL-2 for 3 days in vitro. Anti-IL-2 treatment impaired WT CD8<sup>+</sup> T cell activation as indicated by reduced expression of IFN- $\gamma$  (Supplementary Fig. 4f), Granzyme B, TNF- $\alpha$  and T-bet (Supplementary Fig. 4g), similar as *Trim28*-deficient T cells.

To globally analyze the genes regulated by IL-2 we performed RNA-seq analysis of untreated vs anti-IL-2-treated CD8<sup>+</sup> T cells in the presence of anti-CD3 and anti-CD28 for 3 days in vitro (Supplementary Fig. 4h). Expression of 1656 genes was reduced in anti-IL-2-treated CD8<sup>+</sup> T cells, while that of 1497 genes elevated (Fig. 4e). GO pathway analysis revealed that the gene expression programs following anti-IL-2 treatment were similar to those of *Trim28* deficiency (Figs. 4f, 2g). More importantly, mRNA expression of numerous CD8<sup>+</sup> T cell activation-related surface molecules (*Icos*, *Entpd1*, *Cd69* and etc.), cytotoxicity molecules (*Ifng*, *Gzmb*, *Gzmk* and etc.) and transcriptional factors (*Tbx21*, *Prdm1*, *Id2* and etc.) was significantly downregulated (Fig. 4g). The above results indicated that anti-IL-2 treatment mimicked *Trim28* deficiency, so we overlapped genes downregulated due to *Trim28* deficiency together with those in anti-IL-2-treated activated CD8<sup>+</sup> T cells and extracted a list of 697 genes, including many well-known CD8<sup>+</sup> T cell activation signature genes, such as *Ifng*, *Gzmb*, *Tbx21*, *Il2ra* and *Icos* (Fig. 4h). The overlapped upregulated genes included naive CD8<sup>+</sup> T cell signature genes like *Tcf3*, *Slamf6* and *Id3* (Fig. 4h). Consistent with the above results, GSEA analyses revealed

that the transcriptome of anti-IL-2-treated CD8<sup>+</sup> T cells were relatively more similar with activated *Trim28*<sup>-/-</sup> CD8<sup>+</sup> T cells, which further indicated *Trim28* deficiency impaired CD8<sup>+</sup> T cell activation via limiting IL-2 expression (Fig. 4i).

The interaction of IL-2 and IL-2 receptor activates STAT5 transcription factor, and then STAT5 can regulate expression of genes associated with T cell activation<sup>41</sup>. To confirm that IL-2 signaling is required for CD8<sup>+</sup> T cell function, we isolated naive CD8<sup>+</sup> T cells from WT, *Trim28*<sup>-/-</sup> and *Il2ra*<sup>-/-</sup> mice and conducted T-cell activation in vitro. We found that *Trim28* or *Il2ra* deficiency both impaired the expression of IFN- $\gamma$  (Supplementary Fig. 4i), Granzyme B and TNF- $\alpha$  (Supplementary Fig. 4j). In addition, phosphorylation of STAT5 was also found to be inhibited in *Trim28*<sup>-/-</sup> CD8<sup>+</sup> T cells (Supplementary Fig. 4k). Similarly, treatment with a STAT5 inhibitor reduced the expression of IFN- $\gamma$ , similar to *Trim28* deficiency (Supplementary Fig. 4l).

Overall, the above results indicated that TRIM28 regulates CD8<sup>+</sup> T cell activation via IL-2 production.

### TRIM28 regulates the chromatin accessibility and spatial structure during CD8<sup>+</sup> T cell activation

TRIM28 was previously identified as a co-regulator to recruit chromatin modifiers to regulate gene expression<sup>29,30</sup>. We further explored whether TRIM28 regulates the chromatin accessibility during CD8<sup>+</sup> T cell activation, using ATAC-seq (Supplementary Fig. 5a). In naive CD8<sup>+</sup> T cells, *Trim28* deficiency did not significantly alter chromatin accessibility, consistent with its low expression in naive T cells. Only 39 chromatin regions (0.18%) were altered in naive *Trim28*<sup>-/-</sup> CD8<sup>+</sup> T cell (Fig. 5a). No obvious change in chromatin accessibility was observed in the promoter regions of *Il2*, *Tbx21*, *Ifng* and *Gzmb* in naive *Trim28*<sup>-/-</sup> CD8<sup>+</sup> T cells compared with naive WT cells. In activated CD8<sup>+</sup> T cells, however, ablation of *Trim28* significantly altered the chromatin accessibility. We examined 46,788 chromatin accessible regions across all conditions and searched for chromatin accessible regions that were differentially accessible (Fig. 5b). Overall, in activated *Trim28*<sup>-/-</sup> CD8<sup>+</sup> T cells, 1065 (2.3%) chromatin regions exhibited reduced accessibility than in activated WT CD8<sup>+</sup> T cells, whereas 132 (0.28%) chromatin regions were more accessible (Fig. 5b). 6.2% of differentially accessible chromatin regions between naive WT and activated WT CD8<sup>+</sup> T cells were differentially accessible after TRIM28 deficiency. *Il2*, *Ifng* and *Gzmb* gene loci showed decreased accessibility in activated *Trim28*<sup>-/-</sup> CD8<sup>+</sup> T cells (Fig. 5b, c). naive CD8<sup>+</sup> T cell signature genes, such as *Icosl*, *Cxcr5*, *Ccr7* and *Tcf7*, showed increased accessibility by *Trim28* deficiency (Fig. 5b, Supplementary Fig. 5b). Genome-wide AP-1, JunB and BATF binding was predicted to be impaired in the absence of *Trim28* (Supplementary Fig. 5c). Importantly, peak set enrichment analysis (PSEA) revealed that the epigenetic signatures of naive CD8<sup>+</sup> T cells were strongly associated with activated *Trim28*<sup>-/-</sup> CD8<sup>+</sup> T cells (Fig. 5d). Thus, these results indicated that TRIM28 is crucial in shaping the chromatin accessibility associated with CD8<sup>+</sup> T cell activation.

To examine whether *Trim28* deficiency influences the 3D genome structure in addition to chromatin accessibility during CD8<sup>+</sup> T cell activation, we sorted naive CD8<sup>+</sup> T cells from *Trim28*<sup>fl/fl</sup> and *Trim28*<sup>-/-</sup> mice and treated them with anti-CD3 and anti-CD28 for 3 days in vitro. Then Hi-C assay of naive and activated CD8<sup>+</sup> T cell was performed. High quality interaction maps of activated WT and *Trim28*<sup>-/-</sup> CD8<sup>+</sup> T cells were obtained and investigated (Supplementary Fig. 5d). In activated WT CD8<sup>+</sup> T cells, 46% genomic regions were identified as compartment A, and 54% genomic regions were identified as compartment B. Most genomic regions (97%) remained in the same compartments in activated *Trim28*<sup>-/-</sup> CD8<sup>+</sup> T cells compared with those in activated WT cells (Supplementary Fig. 5e). A total of 1.7% of genomic regions switched from compartment A in activated WT CD8<sup>+</sup> T cells to compartment B in *Trim28*<sup>-/-</sup> cells. 1.3% of genomic regions exhibited the opposite switch from compartment B in activated WT CD8<sup>+</sup> T cells to compartment A in

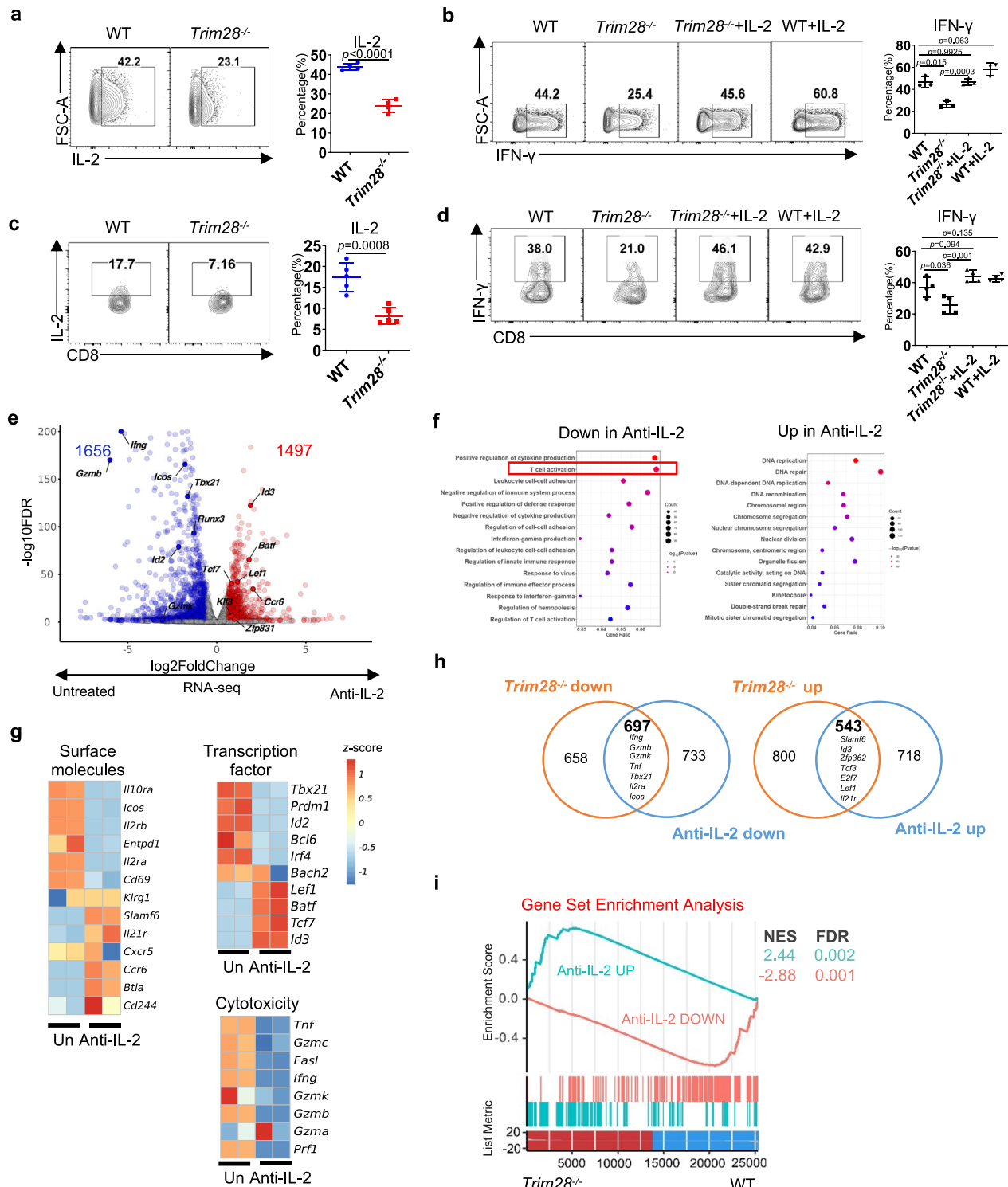
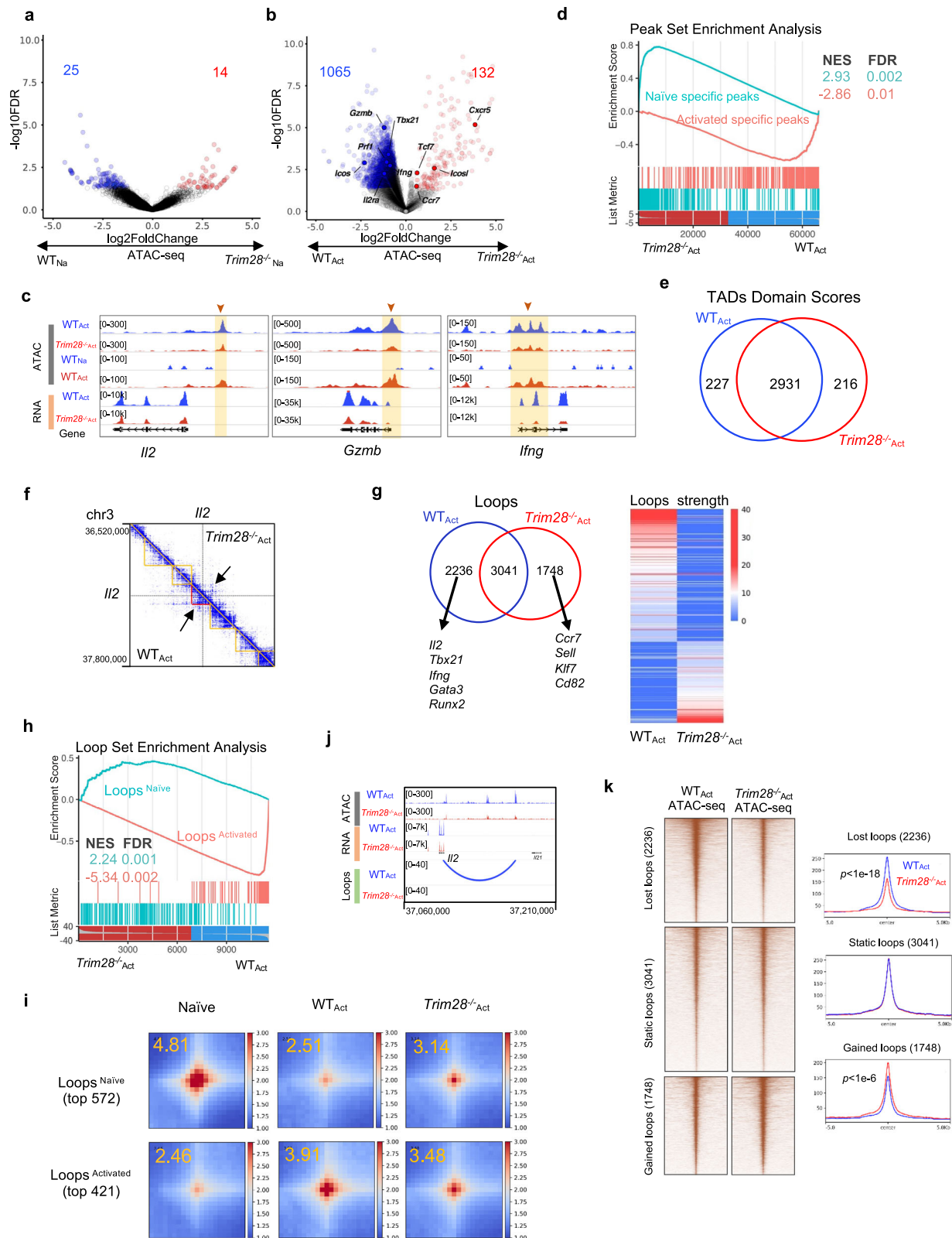


**Fig. 4 | IL-2 treatment could rescue the phenotypes of *Trim28* deficiency.**  
**a** Naive CD8<sup>+</sup> T cells from WT and *Trim28*<sup>-/-</sup> mice were cultured under anti-CD3/28 stimulation for 3 days. Expression of IL-2 was analyzed by flow cytometry.  
**b** Naive CD8<sup>+</sup> T cells from WT and *Trim28*<sup>-/-</sup> mice were cultured with or without IL-2 under anti-CD3/28 stimulation for 3 days. Representative FACS plot showing IFN- $\gamma$  expression.  
**c** *Trim28*<sup>fl/fl</sup>*Cd8 $\alpha$* <sup>Cre</sup> mice and their littermate *Trim28*<sup>fl/fl</sup> mice were infected with LCMV Armstrong virus. IL-2 production by antigen-specific CD8<sup>+</sup> T cells in spleens was measured.  
**d** LCMV Armstrong infected-*Trim28*<sup>fl/fl</sup>*Cd8 $\alpha$* <sup>Cre</sup> mice and their littermate *Trim28*<sup>fl/fl</sup> mice were intraperitoneally injected with or without mIL-2 (10  $\mu$ g per mouse) every two days starting from day 1. Expression of IFN- $\gamma$  by antigen-specific CD8<sup>+</sup> T cells in different groups was measured.  
**e-i** Naive CD8<sup>+</sup> T cells from WT and *Trim28*<sup>-/-</sup> mice were cultured with or without anti-IL-2 under anti-CD3/28 stimulation for 3 days. RNA-seq was conducted after a 3-day culture.

**e** Volcano plot shows transcriptome differences between untreated and anti-IL-2 treated activated CD8<sup>+</sup> T cells. **f** Genes regulated by anti-IL-2 treatment were extracted followed by analysis of and top enriched pathways. **g** Heatmaps illustrating the relative expression of T cell activation signature genes in untreated and anti-IL-2 treated activated CD8<sup>+</sup> T cells. **h** Venn plot of overlapped genes which were upregulated and downregulated by *Trim28*<sup>-/-</sup> activated CD8<sup>+</sup> T cells and anti-IL-2 treated activated CD8<sup>+</sup> T cells. **i** GSEA enrichment of signature genes regulated by anti-IL-2 treatment in the transcriptome of CD8<sup>+</sup> T cells from *Trim28*<sup>fl/fl</sup>*Cd8 $\alpha$* <sup>Cre</sup> mice. Each dot represents one individual replicate ( $n = 3$  per group in **(a, b)**). Each dot represents one individual mouse ( $n = 5$  per group in **(c, d)**,  $n = 4$  per group in **(d)**). Statistical significance was tested by unpaired two-sided Student's *t*-test **(a-d)**. Data are representative of two **(c, d)** and three **(a, b)** independent experiments.



activated *Trim28*<sup>-/-</sup> CD8<sup>+</sup> T cells (Supplementary Fig. 5e). During CD8<sup>+</sup> T cell activation, 11% of the compartment switching from A to B and 15% of compartment switching from B to A were dependent on TRIM28 (Supplementary Fig. 5e). In terms of interactions between compartments, activated *Trim28*<sup>-/-</sup> CD8<sup>+</sup> T cells possessed more intra-B compartment and inter-compartment enrichment compared with activated WT CD8<sup>+</sup> T cells (Supplementary Fig. 5f).

Next, we identified 2501 TADs in activated WT CD8<sup>+</sup> T cells and 2753 TADs in *Trim28*<sup>-/-</sup> cells. Most (75%) of the boundaries of TADs were unchanged in activated WT and *Trim28*<sup>-/-</sup> CD8<sup>+</sup> T cells (Supplementary Fig. 5g). In activated *Trim28*<sup>-/-</sup> CD8<sup>+</sup> T cells, TADs<sup>naive</sup> had increased domain scores and TADs<sup>activated</sup> had decreased domain scores (Supplementary Fig. 5h). Comparing activated *Trim28*<sup>-/-</sup> with activated WT CD8<sup>+</sup> T cells, there were 1060 genes located in 227 TADs with increased

**Fig. 5 | *Trim28* ablation alters the chromatin accessibility and spatial structure in activated CD8<sup>+</sup> T cells.** **a** Volcano plot comparing chromatin accessibility of naive *Trim28*<sup>-/-</sup> CD8<sup>+</sup> T cells (*Trim28*<sup>-/-</sup><sub>Na</sub>) VS naive WT CD8<sup>+</sup> T cells (WT<sub>Na</sub>). The X-axis was the Fold change ( $\log_2$ ) of *Trim28*<sup>-/-</sup> versus WT. Every sample has two replicates. **b** Volcano plot comparing chromatin accessibility of activated *Trim28*<sup>-/-</sup> CD8<sup>+</sup> T cells (*Trim28*<sup>-/-</sup><sub>Act</sub>) VS activated WT CD8<sup>+</sup> T cells (WT<sub>Act</sub>). The X-axis was the Fold change ( $\log_2$ ) of *Trim28*<sup>-/-</sup> versus WT. Every sample has two replicates. **c** Mean ATAC-seq coverage at the *Il2*, *Gzmb* and *Ifng* genes. **d** Chromatin regions specifically accessibility in naive WT CD8<sup>+</sup> T cells (blue) and activated WT CD8<sup>+</sup> T cells (red) were analyzed for enrichment in the activated *Trim28*<sup>-/-</sup> CD8<sup>+</sup> T cells versus activated WT CD8<sup>+</sup> T cells by peak set enrichment analysis (PSEA). **e** Venn diagram of TADs of activated WT and activated *Trim28*<sup>-/-</sup> CD8<sup>+</sup> T cells based on domain scores. TADs, topologically associating domains. Two replicates were analyzed separately to assess consistency, and results were then combined. Details see methods. **f** Hi-C interaction matrix of the regions in activated WT and activated *Trim28*<sup>-/-</sup> CD8<sup>+</sup> T cells

around the *Il2* gene. **g** Venn diagram of chromatin loops of activated WT and activated *Trim28*<sup>-/-</sup> CD8<sup>+</sup> T cells (left). Heatmap of loop strength difference (right). Two replicates were analyzed separately to assess consistency, and the results were then combined. For details see methods. **h** Chromatin specifically loops in naive WT (blue) and activated WT CD8<sup>+</sup> T cells (red) were analyzed for enrichment in the activated *Trim28*<sup>-/-</sup> CD8<sup>+</sup> T cells VS activated WT CD8<sup>+</sup> T cells by loop set enrichment analysis (LSEA). **i** APA (aggregate peak analysis) plot for the selected Loops<sup>naive</sup> and selected Loops<sup>Activated</sup> (loop strength > 30) in naive, activated WT and activated *Trim28*<sup>-/-</sup> CD8<sup>+</sup> T cells. **j** Genome browser view of chromatin accessibility, gene expression and 3D genome interactions around the *Il2* gene in activated WT and activated *Trim28*<sup>-/-</sup> CD8<sup>+</sup> T cells. **k** Heatmaps displaying chromatin accessibility of loop anchors of three types of loops in activated WT and activated *Trim28*<sup>-/-</sup> CD8<sup>+</sup> T cells. Statistical significance was tested by unpaired two-tailed Student's t test (**i**) and Chi-squared test (**k**).

domain scores, such as *Sell*, *Ccr7* and *Tcf7*, and 597 genes located in 216 TADs with decreased domain scores, such as *Il2*, *Tbx21* and *Ifng* (Fig. 5e, f, Supplementary Fig. 5h). The domain score of the TAD where *Il2* is located was decreased by 38% in activated *Trim28*<sup>-/-</sup> compared with activated WT CD8<sup>+</sup> T cells (Fig. 5f). Similarly, the domain scores of the TADs where *Tbx21* and *Ifng* are located were decreased after *Trim28* deficiency (Supplementary Fig. 5i). On the contrary, the domain score of the TAD where *Ccr7* is located was increased in *Trim28*<sup>-/-</sup> activated CD8<sup>+</sup> T cells (Supplementary Fig. 5i).

We identified 2236 unique chromosomal loops, defined as lost loops, in activated WT CD8<sup>+</sup> T cells and 1748 in *Trim28*<sup>-/-</sup> T cells, defined as gained loops, with 3041 in both lists which were defined as static loops (Fig. 5g). Globally, loop set enrichment analysis (LSEA) revealed that the epigenetic signatures (572 loops) of naive CD8<sup>+</sup> T cells were strongly enriched in activated *Trim28*<sup>-/-</sup> CD8<sup>+</sup> T cells, based on the Hi-C data (Fig. 5h). During CD8<sup>+</sup> T cell activation, 47% of Loops<sup>Activated</sup> and 5% of Loops<sup>naive</sup> were dependent on TRIM28. The APA enrichment score of Loops<sup>naive</sup> in activated *Trim28*<sup>-/-</sup> CD8<sup>+</sup> T cells was higher than that in activated WT cells, whereas the APA enrichment score of Loops<sup>Activated</sup> in activated *Trim28*<sup>-/-</sup> CD8<sup>+</sup> T cells was lower than that in activated WT cells (Fig. 5i), which indicated that *Trim28* may mediate the chromatin loops associated with T cell activation. 536 genes located in the lost loop anchor regions in activated *Trim28*<sup>-/-</sup> CD8<sup>+</sup> T cells, such as *Ifng*, *Tbx21*, *Fli1*, *Slamf7*, *Ccnd2* and *Cdc6*, were enriched in the pathways in regulation of T cell activation and cell cycles by GO terms. 317 genes located in the gained loop anchor regions in activated *Trim28*<sup>-/-</sup> CD8<sup>+</sup> T cells, such as *Myc*, *Rif1*, *Cbx7*, *Msl3* and *Suz12* were enriched in pathways of chromatin organization and chromatin modifying enzymes (Supplementary Fig. 6a).

The above results have indicated that TRIM28 was necessary for the chromosomal looping associated with T cell activation and function in CD8<sup>+</sup> T cells. Specifically, in activated WT CD8<sup>+</sup> T cells, there was a significant loop (78 kb) between the *Il2* promoter and an upstream chromatin accessible region (442 bp, Fig. 5j). However, this loop disappeared in activated *Trim28*<sup>-/-</sup> CD8<sup>+</sup> T cells (Fig. 5k). The 3C experiments showed that the interaction strength of this loop was decreased significantly after *Trim28* deficiency in activated CD8<sup>+</sup> T cells, suggesting our Hi-C results were reliable (Supplementary Fig. 6b–d). Similarly, the loop strengths of the loops where *Tbx21* and *Ifng* are located were decreased in the absence of *Trim28* (Supplementary Fig. 6e). On the contrary, the loop strength of the loops where *Ccr7* is located was increased in activated *Trim28*<sup>-/-</sup> CD8<sup>+</sup> T cells (Supplementary Fig. 6e). Moreover, the loops strengths where the 358 T-cell activation genes<sup>34</sup> are located were decreased in activated *Trim28*<sup>-/-</sup> CD8<sup>+</sup> T cells (Supplementary Fig. 6f). These results indicated a key role for TRIM28 in 3D genome re-organization associated with CD8<sup>+</sup> T cell activation. At the same time, these changes in the 3D structure of chromatin were also accompanied by changes in chromatin accessibility. We also examined the accessibility of loop anchors. The

chromatin accessibilities of lost loop anchors were decreased while the chromatin accessibilities of gained loop anchors increased in activated *Trim28*<sup>-/-</sup> CD8<sup>+</sup> T cells (Fig. 5k).

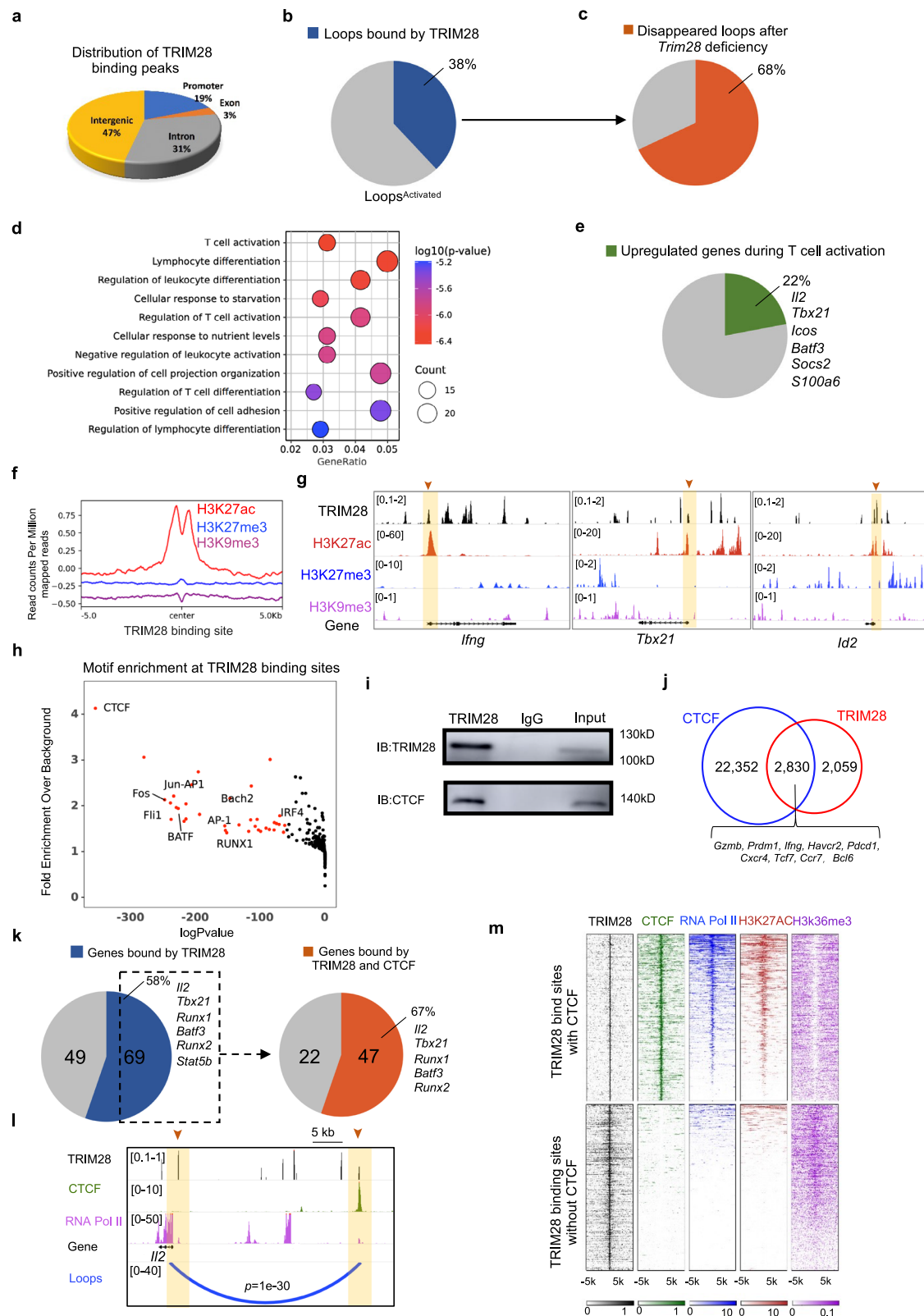
Taken together, these results indicate that TRIM28 is required for reconfiguration of the chromatin accessibility and spatial structure during CD8<sup>+</sup> T cell activation.

### TRIM28 and CTCF are co-localized at the signature genes of T cell activation

To investigate the mechanism by which TRIM28 regulates the target genes, we performed chromatin immunoprecipitation-coupled with high-throughput sequencing (ChIP-seq) analysis using in vitro activated CD8<sup>+</sup> T cells to determine the genome-wide occupancy of TRIM28. Results showed that TRIM28 binding was mainly enriched in the promoter (19% of TRIM28 binding peaks *vs.* 2% of the mouse whole genome, 3 kb upstream and downstream of the transcription start site) and intron regions (31% *vs.* 20% of the mouse whole genome) (Fig. 6a). Comparison of TRIM28-bound with TRIM28-regulated genes revealed that 2158 out of 8262 TRIM28-bound genes were transcriptionally regulated by TRIM28, including *Ifng*, *Icos*, *Tbx21*, *Tcf7*, *Lef1* and *Il2* (Supplementary Fig. 7a). 1197 peaks were differentially accessible between activated WT and activated *Trim28*<sup>-/-</sup> CD8<sup>+</sup> T cells (Fig. 5b). 34.5% of differentially accessible chromatin regions were bound by TRIM28, such as *Ifng*, *Tbx21* and *Il2* (Supplementary Fig. 7b). Specifically, TRIM28 binding was identified in the promoter and/or intron regions of the *Ifng*, *Tbx21* and *Il2* genes (Supplementary Fig. 7c).

The accessibilities of most TRIM28 binding sites were decreased in activated *Trim28*<sup>-/-</sup> CD8<sup>+</sup> T cells compared to WT cells (Supplementary Fig. 7d). 38% (543) of Loops<sup>Activated</sup> were bound by TRIM28, 68% (371) of which disappeared after *Trim28* deficiency in activated state (Fig. 6b, c). 530 genes located in the 371 TRIM28 dependent loops, were enriched in GO terms related to T cell activation and regulation of T cell activation (Fig. 6d). Moreover, the expression of 115 genes in the 530 genes were significantly upregulated (fold change > 2, *p*-value < 1e-3) during CD8<sup>+</sup> T cell activation, such as *Il2*, *Tbx21*, *Icos*, *Batf3* (Fig. 6e).

TRIM28 was widely regarded as a co-repressor through associating with the H3K9me3-writer SETDB1/ESET and histone deacetylation complex NuRD to form heterochromatin<sup>42,43</sup>. However, TRIM28 was also previously reported as a positive regulator in Th17 cells<sup>25</sup>. Then we performed H3K27ac ChIP-seq in activated WT and activated *Trim28*<sup>-/-</sup> CD8<sup>+</sup> T cells. There were 7013 H3K27ac-associated sites in activated *Trim28*<sup>-/-</sup> CD8<sup>+</sup> T cells but 4598 in WT cells (Supplementary Fig. 7e). *Trim28* deficiency resulted in reduction of H3K27ac signals in many T cell activation-related genes, such as *Ifng*, *Gzmb* and *Id2* implicating that TRIM28 promotes CD8<sup>+</sup> T cell activation (Supplementary Fig. 7e). Specifically, H3K27ac ChIP-qPCR results showed that the presence of H3K27ac at the *Ifng*, *Gzmb* and *Id2* genes was significantly reduced after *Trim28* deficiency (Supplementary Fig. 7f). TRIM28 binding peaks were largely co-localized with H3K27ac marks, but not with repressive



H3K27me3<sup>44</sup> and H3K9me3<sup>45</sup> marks in CD8<sup>+</sup> T cells (Fig. 6f). Specifically, TRIM28 binding was identified in the promoter and/or intron regions of the *Ifng*, *Tbx21* and *Id2* genes, which were largely co-localized with active histone modifications in effector CD8<sup>+</sup> T cells<sup>44</sup> (Fig. 6g). We also found that the accessibility and active histone modifications at these locations were reduced in the absence of *Trim28* (Supplementary Fig. 7g). These results suggest that TRIM28 may

positively regulate gene transcription via binding to enhancers. Moreover, we found that the H3K27ac modification at lost loop anchors were decreased while the H3K27ac modification of gained loop anchors increased in activated *Trim28*<sup>-/-</sup> CD8<sup>+</sup> T cells, compared with WT cells (Supplementary Fig. 7h and i). This indicates that the changes in the 3D structure of chromatin also correlated with the changes in H3K27ac modification. Furthermore, a significant decrease

**Fig. 6 | TRIM28 and CTCF exhibit co-localization in activated CD8<sup>+</sup> T cell genome.** **a** Distribution of TRIM28 binding peaks in activated WT CD8<sup>+</sup> T cells. **b** Proportions of loops<sup>Activated</sup> occupied by TRIM28 in activated CD8<sup>+</sup> T cell. **c** Proportions of loops disappeared after *Trim28* deficiency in the loops<sup>Activated</sup> bound by TRIM28. **d** Gene ontology enrichment analysis for the 530 genes located in the anchor regions of the loops in (c). **e** Proportions of upregulated genes during CD8<sup>+</sup> T cell activation in the 530 genes located in the anchor regions of the loops in (c). **f** Aggregate plot of H3K27ac, H3K27me3 and H3K9me3 modification at  $\pm 5.0$  Kb in CD8<sup>+</sup> T cells of the TRIM28 binding sites in activated WT CD8<sup>+</sup> T cells. **g** Genome browser views showing TRIM28 binding sites and histone modifications around *Irfng*, *Tbx21* and *Id2* in activated WT CD8<sup>+</sup> T cells determined using ChIP-seq data. **h** Motif enrichment analysis in the TRIM28 binding sites. **i** Co-immunoprecipitation (IP) of CTCF by an anti-TRIM28 antibody in the activated WT CD8<sup>+</sup> T cells. **j** Venn

diagram showing the overlap between CTCF peaks (blue) and TRIM28 peaks (red) in activated WT CD8<sup>+</sup> T cells. **k** Proportions of WT<sub>Na</sub> vs. WT<sub>Act</sub> specific genes occupied by TRIM28 in activated state (left). Proportions of WT<sub>Na</sub> vs. WT<sub>Act</sub> specific genes both occupied by TRIM28 and CTCF in activated state (right). **l** Genome browser view of TRIM28, CTCF, RNA Pol II binding signals and 3D genome interactions around the *Il2* gene in activated WT CD8<sup>+</sup> T cells. **m** Heatmap displaying TRIM28, CTCF, H3K27ac and RNA Pol II at TRIM28 binding sites in activated WT CD8<sup>+</sup> T cells using ChIP-seq and CUT&Tag data. The upper panel showed the TRIM28 binding sites with CTCF in activated WT CD8<sup>+</sup> T cells. The lower panel showed the TRIM28 binding sites without CTCF in activated WT CD8<sup>+</sup> T cells. Statistical significance was tested by Chi-squared test (**b**), unpaired two-tailed Student's t test (**c**) and hypergeometric test (**j**). Data are representative of two (**i**) independent experiments.

in H3K27ac modification at CD8<sup>+</sup> T cell-specific enhancers was observed in the absence of TRIM28, especially those occupied by TRIM28 (Supplementary Fig. 7j and k). This suggests that CD8<sup>+</sup> T cell-specific enhancers may be positively regulated by TRIM28.

T cell activation-related TFs, such as Fos, Fli1 and BATF exhibited increased binding to TRIM28-occupied sites in activated CD8<sup>+</sup> T cells (Fig. 6h). However, CTCF showed the highest correlation. This result suggested that TRIM28 may be directly involved in the regulation of chromatin spatial structure, as CTCF is the master regulator of 3D genome organization<sup>4</sup>. Co-IP experiment further validated the interaction of TRIM28 and CTCF in activated CD8<sup>+</sup> T cells (Fig. 6i). To investigate whether TRIM28 cooperates with CTCF to regulate target genes through 3D genome, we performed CTCF CUT&Tag experiment to evaluate the co-localization of TRIM28 and CTCF. There was a significant overlap between the CTCF and TRIM28 occupancy in the genome of activated CD8<sup>+</sup> T cells, as shown by Venn diagram (Fig. 6j). We analyzed the proportions of T cell activation genes in differentially regulated loops after TRIM28 deficiency in activated T cells. 33% T cell activation signature genes were located in lost loops after TRIM28 deficiency, among which 58% had TRIM28 binding sites (Fig. 6k), indicative of direct regulation by TRIM28. Moreover, 67% TRIM28 bound-T cell activation signature genes were also occupied by CTCF (Fig. 6k). For example, the binding of TRIM28 and CTCF was co-localized in the *Il2* gene (Fig. 6l). We then divided genome-wide TRIM28-bound regions into two categories: co-localized with CTCF (cluster 1) and not (cluster 2). There were 2145 genes in cluster 1 such as *Il2*, *Tcf7*, *Icos*, *Foxo3*, *Tbx21*, *Havcr2* and *Tigit*, which are related to T cell activation and IL-2 signaling pathways. 1834 genes were in cluster 2 such as *Atf1*, *Creb1*, *Map2k4*, *Map3k8*, *Tab2*, *Gata3*, *Il4* and *Card11* enriched in MAP kinase activation and T cell selection pathways (Supplementary Fig. 7l). Previous studies reported that TRIM28 could interact with RNA polymerase (Pol) II to regulate gene expression<sup>32</sup>. RNA Pol II could cooperate with CTCF to arrange the spatial organization for coordinated transcription<sup>46</sup>. We found TRIM28-associated sites in Cluster 1 genes correlated with RNA Pol II binding<sup>47</sup> and H3K27ac modification. In contrast, cluster 2 genes were correlative with H3K36me3 modification<sup>48</sup>, but not binding of RNA Pol II or H3K27ac marks (Fig. 6m, Supplementary Fig. 7m). This strongly indicates that TRIM28 binding in the Cluster 1 genes was involved in the transcriptional activation of genes and the regulation of chromatin spatial conformation. On the other hand, its binding in the Cluster 2 genes was mainly in the gene body regions and may be mainly involved in the transcriptional elongation regulation, consistent with a previous study<sup>32</sup>. At the same time, CTCF and TRIM28 co-localized sites had increased histone modification of H3K27ac and accessibilities, suggesting that TRIM28 and CTCF cooperate in positive regulation of gene transcription, possibly via 3D genome organization (Supplementary Fig. 7n).

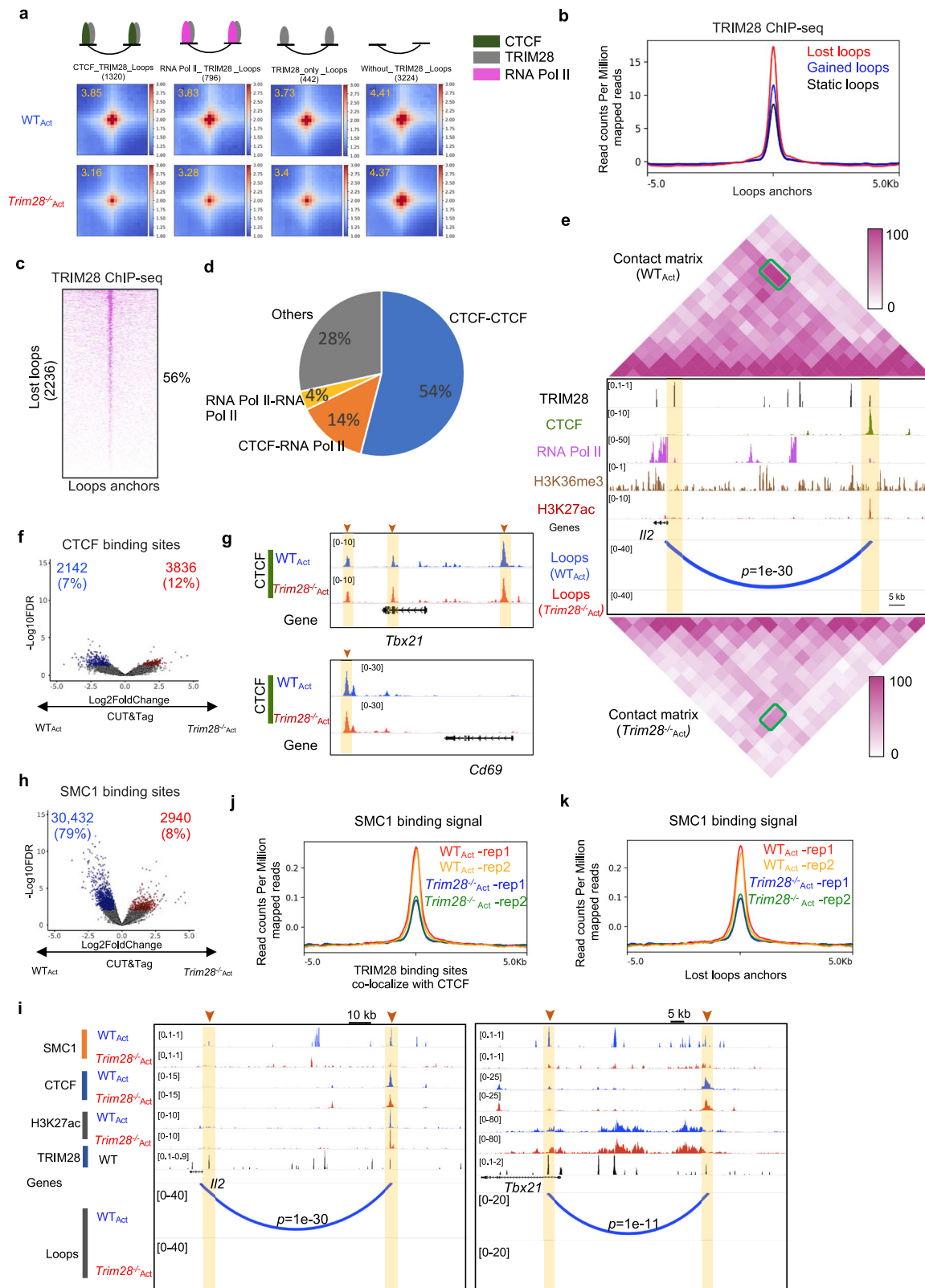
### TRIM28, CTCF, RNA Pol II and cohesin cooperate to shape chromosomal interactions during CD8<sup>+</sup> T cell activation

The above results indicate that TRIM28 may positively regulate the transcription of T cell activation genes together with CTCF. To explore

how TRIM28 regulates the expression of target genes by affecting the spatial structure of chromatin, we divided all chromatin loops into four categories according to the protein binding in the loop anchors region: CTCF\_TRIM28\_Loops, RNA Pol II\_TRIM28\_Loops, TRIM28\_only\_Loops and without\_TRIM28\_Loops. The first three types of loops had significant reductions in loop strengths in activated *Trim28*<sup>-/-</sup> CD8<sup>+</sup> T cells compared with WT cells (Fig. 7a). This indicated that *Trim28* deficiency significantly affected the formation of chromosomal loops, especially those mediated by CTCF and RNA Pol II. In Fig. 5h, we defined the loops that were lost, gained or static in activated CD8<sup>+</sup> T cells after *Trim28* deficiency. To explore whether TRIM28 was directly involved in chromatin looping, we investigated the binding signal of TRIM28 in the anchor regions of these three types of loops. The ChIP-seq data indicated that TRIM28 binding was more significant ( $p < 0.01$ , Chi-squared test) in the anchor regions of the lost loops than in the gained loops and static loops (Fig. 7b). 56% (1252) of lost loops had direct binding of TRIM28 in the anchor regions. (Fig. 7c).

Next, we divided these lost loops (2236) into four categories according to whether CTCF and RNA Pol II bound to the loop anchor regions (Fig. 7d). Among them, the loop where *Il2* was located belonged to the CTCF-RNA Pol II group, whose length was about 78 kb (Fig. 7e). The loop anchor on the upstream side of this loop was the promoter of *Il2* with significant occupancy by TRIM28 and RNA Pol II, while the downstream loop anchor was an enhancer, bound by both TRIM28 and CTCF and with H3K27ac marks (Fig. 7e). Pathway enrichment analysis showed that 583 genes located in CTCF-RNA Pol II loops were related to T cell activation, such as *Tbx21* and *Runx2* (Supplementary Fig. 8a, b). 1134 genes located in CTCF-CTCF loops were involved in T cell proliferation, such as *Cxcr4*, *Socs3* and *Ccl3* (Supplementary Fig. 8a, c). 175 genes located in RNA Pol II-RNA Pol II loops were involved in signaling by interleukins, such as *Il7r* and *Ripk2* (Supplementary Fig. 8a, d).

However, a small subset of TRIM28-associated loops, which lacked CTCF and/or RNA Pol II binding (442 TRIM28\_only loops in Fig. 7a), exhibited significant enrichment in the *Trim28*<sup>-/-</sup>Act contact map. This suggested that other proteins might be involved in regulating these loops. The anchor regions of TRIM28\_only\_Loops exhibited strong enrichment of T cell activation-related TFs, such as BATF, Fos and AP-1 (Supplementary Fig. 8e). BATF was reported to regulate the expression of genes associated with effector programs, such as *Fos*, *Ctla4*, *Maf*, *Il12rb2*, *Hif1a*, and *Itga4* by facilitating the formation of chromatin loops around these genes in CD8<sup>+</sup> T cells during acute infection<sup>49</sup>. Genes associated with effector function including *Icos*, *Ctla2b*, *Maf*, *Il12rb2*, *Hif1a*, and *Itga4* were located in the TRIM28\_only\_Loops. Further analysis showed that BATF was enriched in the chromatin accessibility regions within the loop anchor of TRIM28\_only\_Loops (Supplementary Fig. 8f). At the same time, there was a significant overlap between the BATF and TRIM28 occupancy at the TRIM28 binding sites within the loop anchor of TRIM28\_only\_Loops in activated WT CD8<sup>+</sup> T cells, as shown by heatmap (Supplementary Fig. 8g). This suggests TRIM28 may cooperate with BATF to mediate



loops formation to regulate the expression of genes associated with effector programs, but not those associated with T cell activation, since *Batf* deficiency did not affect these genes, IL-2 included, in their expression<sup>49</sup>.

Previous studies reported CTCF and cohesin cooperate to mediate loops formation<sup>3,4,6</sup>. Considering the close association of TRIM28 and CTCF, we firstly explored their recruitment mechanisms. *Trim28*

deficiency did not significantly affect the binding of CTCF in the whole genome (Fig. 7f, Supplementary Fig. 8h), such as at the *Tbx21*, *Pdcd1* and *Cd69* enhancer (Fig. 7g, Supplementary Fig. 8i). Next, we investigated whether CTCF recruit TRIM28. CTCF was knocked out in activated CD8<sup>+</sup> T cells using CRISPR-Cas9 (Supplementary Fig. 8j). TRIM28 CUT&Tag experiment were performed in WT and CTCF-deficient CD8<sup>+</sup> T cells. A significant decrease in TRIM28 binding signal at TRIM28

**Fig. 7 | TRIM28 regulates target genes by mediating the chromatin loops.** **a** APA plot showing the CTCF\_TRIM28\_Loops, RNA Pol II\_TRIM28\_Loops, TRIM28\_only\_Loops and without\_TRIM28\_Loops in activated WT and activated *Trim28*<sup>-/-</sup> CD8<sup>+</sup> T cells. **b** Aggregate plot showing TRIM28 binding signal at the loop anchors of lost, gain and static loops. **c** Heatmap displaying TRIM28 binding signal at the loop anchors of lost loops. **d** The percentage of different loop types in all lost loops in activated *Trim28*<sup>-/-</sup> CD8<sup>+</sup> T cells compared to activated WT cells. **e** Genome browser views showing TRIM28, CTCF, RNA Pol II binding sites, H3K27ac, H3K36me3 modification and 3D genome interactions around *Il2* in activated WT and activated *Trim28*<sup>-/-</sup> CD8<sup>+</sup> T cells. **f** Volcano plot comparing binding signal of CTCF between activated *Trim28*<sup>-/-</sup> CD8<sup>+</sup> T cells VS WT CD8<sup>+</sup> T cells. The X-axis was the Fold change (log<sub>2</sub>) of activated *Trim28*<sup>-/-</sup> versus activated WT. FDR ≤ 0.01 and FC ≥ 1.5. **g** Genome browser views showing CTCF binding signal around *Tbx21* and *Cd69* in activated WT and activated *Trim28*<sup>-/-</sup> CD8<sup>+</sup> T cells. **h** Volcano plot comparing binding signal of

SMC1 between activated *Trim28*<sup>-/-</sup> CD8<sup>+</sup> T cells VS WT CD8<sup>+</sup> T cells. The X-axis was the Fold change (log<sub>2</sub>) of activated *Trim28*<sup>-/-</sup> versus activated WT. FDR ≤ 0.01 and FC ≥ 1.5. **i** Genome browser views showing SMC1 CTCF, TRIM28 binding sites, H3K27ac, modification and 3D genome interactions around *Il2* and *Tbx21* in activated WT and activated *Trim28*<sup>-/-</sup> CD8<sup>+</sup> T cells. **j** Aggregate plot displaying SMC1 binding signal at the TRIM28 binding sites co-localize with CTCF in activated WT and activated *Trim28*<sup>-/-</sup> CD8<sup>+</sup> T cells. The binding of SMC1 at the binding sites of TRIM28 were significantly higher in activated WT CD8<sup>+</sup> T cells than in *Trim28*<sup>-/-</sup> cells ( $p < 1e-16$ ). **k** Aggregate plot of SMC1 binding signal at the lost loops anchors in activated WT and activated *Trim28*<sup>-/-</sup> CD8<sup>+</sup> T cells. The binding of SMC1 at the lost loop anchor regions were significantly higher in activated WT CD8<sup>+</sup> T cells than in *Trim28*<sup>-/-</sup> cells ( $p < 1e-16$ ). Statistical significance was tested by unpaired two-tailed Student's t test (**a**) and Chi-squared test (**b**, **j** and **k**).

binding sites, especially those co-localized with CTCF (Supplementary Fig. 8k), such as in the promoter regions of *Il2*, *Ifng*, *Tbx21* and *Cd69* was observed in CTCF-deficient CD8<sup>+</sup> T cells (Supplementary Fig. 8l). These results suggest that CTCF recruit TRIM28.

Previous studies reported that cohesin mediates the loops formation and promotes the loop strength<sup>5,50–52</sup>. A decrease in cohesin binding results in the disappearance of the loops and the reduction in loop strength<sup>5,50–52</sup>. Then, we explored the association between TRIM28 and cohesin. Co-IP experiments demonstrated that TRIM28 could form a complex with SMC1 a cohesin subunit, in activated CD8<sup>+</sup> T cells (Supplementary Fig. 8m). Next, we performed CUT&Tag analysis with antibodies for SMC1 in activated WT and activated *Trim28*<sup>-/-</sup> CD8<sup>+</sup> T cells (Supplementary Fig. 8n). The binding of SMC1 was significantly reduced in the whole genome by *Trim28* deficiency (Fig. 7h). Specifically, we found that SMC1 binding was significantly decreased at the *Il2* and *Tbx21* loci in the absence of *Trim28* (Fig. 7i), which were identified by ChIP-qPCR (Supplementary Fig. 8o). Meanwhile, the chromatin loops where *Il2* and *Tbx21* are located disappeared after *Trim28* deficiency (Fig. 7i). Therefore, the reduction in SMC1 binding resulting from *Trim28* deletion has an impact on the loop strength. Moreover, we found cohesin and TRIM28 co-localized with CTCF (Fig. 7j, Supplementary Fig. 8p). Especially, the binding of SMC1 at the binding sites of TRIM28 and the lost loop anchor regions were significantly higher in activated WT CD8<sup>+</sup> T cells than in activated *Trim28*<sup>-/-</sup> cells (Fig. 7j, k), suggesting that TRIM28 may recruit cohesin and facilitate the binding of cohesin at the CTCF binding sites.

Taken together, TRIM28 acts as a mediator that together with CTCF, cohesin and RNA Pol II regulates chromosomal loop formation at genes related to T cell activation (Supplementary Fig. 9a).

## Discussion

In the current work, we described the 3D genome changes during CD8<sup>+</sup> T cell activation and identified a crucial role of TRIM28 in regulating CD8<sup>+</sup> T cell activation by mediating the accessibility and spatial structure of chromatin. *Trim28* deficiency impaired CD8<sup>+</sup> T cell activation in vitro and in vivo, which was mainly due to its regulation of IL-2 production. Mechanistically, TRIM28 regulated the transcription of target genes by cooperating with CTCF, RNA Pol II and cohesin to mediate the formation of chromatin loops.

Several transcription factors were reported to facilitate enhancer-promoter loop formation to regulate gene transcription in CD8<sup>+</sup> T cells. Tcf1 and CTCF cooperatively shape genomic architecture to promote CD8<sup>+</sup> T cell homeostasis<sup>53</sup>. BATF-mediated epigenetic control of effector CD8<sup>+</sup> T cell differentiation<sup>49</sup>. However, these studies mainly investigated the chromatin interactions mediated by specific transcription factors, whereas 3D chromatin conformation at the genome levels during CD8<sup>+</sup> T cell activation has not been systematically illustrated. In this study, we found that activated CD8<sup>+</sup> T cells had significant changes in the 3D genome and chromatin accessibility. During CD8<sup>+</sup> T cell activation, 6.9% A/B compartments, 24% TADs, and 85%

loops were reorganized. These changes in the 3D genome were closely related to the transcription of T cell activation genes, such as *Il2*, *Ifng* and *Tbx21*. Furthermore, our analysis of *Trim28*-deficient mice has revealed the importance of 3D genome in T cell activation and function. To our knowledge, this work systematically characterized the 3D genome reorganization at compartment, TAD and loop levels during CD8<sup>+</sup> T cell activation.

Multiple studies have reported that TRIM family proteins can act as epigenetic modifiers to regulate gene expression<sup>28–30</sup>. A member in this family, TRIM28, was found to be highly expressed in activated CD8<sup>+</sup> T cell compared with naive CD8<sup>+</sup> T cell. Previous reports have suggested that TRIM28 plays a critical role in Th17 and Treg cell differentiation<sup>25,54</sup>. In the current study, we first found TRIM28 is required for CD8<sup>+</sup> T cell activation. *Trim28* deficiency led to deficits in *Ifng*, *Gzmb*, *Tbx21* and *Cd69* expression and greatly increased *Id3* and *Tcf7* expression during CD8<sup>+</sup> T cell activation, closely phenocopying naive CD8<sup>+</sup> T cells. Genetic ablation of *Trim28* impaired the anti-tumor and anti-infection functions of activated CD8<sup>+</sup> T cells in vivo. The expression of immune checkpoints PD-1, TIM-3, TIGIT and CTLA-4 was not affected after *Trim28* deficiency (Supplementary Fig. 9b–e), which indicates that the anti-tumor function of TRIM28 is not associated with immune checkpoint regulation. In cancer and chronic infection, persistent antigenic stimulation drives CD8<sup>+</sup> T cells into an exhaustion state. Exhausted CD8<sup>+</sup> T cells are heterogenous and have been mainly classified into two populations, named progenitors (Tex<sup>pro</sup>) and terminally exhausted CD8<sup>+</sup> T cells (Tex<sup>ter</sup>)<sup>55,56</sup>. Tex<sup>ter</sup> cells, with characteristics of potent cytotoxicity and high-level apoptosis, highly express *Havcr2*, *Entpd1*, *Ifng*, *Gzmb* and *Tbx21*<sup>55,56</sup>. In contrast, Tex<sup>pro</sup> cells are stem-like and highly express *Tcf7*, *Lef1*, *Id3* and *Slamf6*, which can proliferate and differentiate into Tex<sup>ter</sup> cells<sup>55,56</sup>. In tumor, the expression of Tex<sup>ter</sup> characteristic molecules were decreased in CD8<sup>+</sup> TILs after *Trim28* deficiency, suggesting that *Trim28*<sup>-/-</sup> CD8<sup>+</sup> TILs were similar to Tex<sup>pro</sup> cells. Further studies are needed to explore the role of TRIM28 in exhausted CD8<sup>+</sup> T cell.

Some TRIM family members like *Trim16*, *Trim37*, *Trim46* and *Trim27* expression was also found to be substantially elevated in activated CD8<sup>+</sup> T cells, as compared to naive CD8<sup>+</sup> T cells. TRIM27 was reported to negatively regulate CD4<sup>+</sup> T cell activation<sup>57</sup>. *TRIM37* mutations was associated with a selective impairment in the numbers and function of CD4<sup>+</sup> T cells<sup>58</sup>. As for TRIM16 and 46, there has been no study reporting their roles in T cells. The roles of these genes in the activation of CD8<sup>+</sup> T cells need to be further identified.

Previous studies reported that TRIM28 functions as a transcriptional co-repressor by recruiting repressive epigenetic complexes to induce chromatin condensation<sup>43,59</sup>. However, our analysis of ChIP-seq data in CD8<sup>+</sup> T cells revealed that genome-wide binding of TRIM28 highly correlated with active epigenetic marker H3K27ac, but not with repressive H3K9me3 and H3K27me3 marks in CD8<sup>+</sup> T cells. Genetic ablation of *Trim28* resulted in a global reduction of H3K27ac levels. In total, *Trim28* deficiency affected the expression of total 2602 genes in

CD8<sup>+</sup> T cells: expression of 1190 (45.7%) was reduced in *Trim28*-deficient CD8<sup>+</sup> T cells, among which 44% contain TRIM28 binding sites, whereas 1412 (54.3%) genes had increased expression with less than 34% of them having TRIM28 binding. These data together suggest that TRIM28 largely functions as an epigenetic co-activator in CD8<sup>+</sup> T cell activation, consistent to our previous analysis on TRIM28 function in Th17 cells<sup>25</sup>. TRIM28 was largely identified as a transcriptional cofactor, by recruiting epigenetic complexes and interacting with transcription factors, or through ubiquitin E3 activity<sup>60</sup>. Further studies are needed to explore whether TRIM28 regulate CD8<sup>+</sup> T cell activation depending on its enzyme activity.

TRIM28 also acts as a transcriptional elongation factor to regulate gene expression<sup>32</sup>. Our analysis of ChIP-seq data demonstrated that although TRIM28 binding sites were largely co-localized with those of CTCF in activated CD8<sup>+</sup> T cells, TRIM28 occupancy that do not co-localize with CTCF may function in transcriptional elongation, evidenced by their co-localization with H3K36me3 an epigenetic marker for transcriptional elongation<sup>61,62</sup>. Previous studies found TRIM28 was critical for release of RNA Pol II from its paused state. TRIM28 knock-down significantly decreased H3K36me3 modification<sup>63</sup>. TRIM28 co-occupancy with H3K36me3 likely regulates gene expression by transcriptional elongation during CD8<sup>+</sup> T cell activation.

TRIM28 co-occupancy with CTCF likely regulates gene expression by forming TADs and chromatin loops with CTCF. Indeed, in the absence of *Trim28*, 3% of A/B compartments, 15% of TADs and 41% of loops had significant changes. *Trim28* deficiency had a greater impact on the level of loop structure than TADs and A/B compartments. 38% (543) of Loops<sup>Activated</sup> were bound by TRIM28, 68% (371) of which disappeared after *Trim28* deficiency in activated state. This low number of affected loops bound by TRIM28 might indicate indirect effects of *Trim28* deficiency in chromatin looping. Importantly, Co-IP experiments demonstrated that TRIM28 formed a complex with CTCF in activated CD8<sup>+</sup> T cells. Meanwhile, a significant decrease in TRIM28 binding signal at TRIM28 binding sites was observed in CTCF-deficient CD8<sup>+</sup> T cell. These results suggest that TRIM28 might be recruited by CTCF since TRIM28 cannot directly bind to DNA.

TADs and loops are partitioned into self-interacting blocks by cohesin and CTCF<sup>2,3,64</sup>. The binding of CTCF in the whole genome were mostly unchanged between activated WT and activated *Trim28*<sup>-/-</sup> CD8<sup>+</sup> T cells. Cohesin was thought to form TADs and loops by extruding chromatin loops until blocked by CTCF boundaries, thereby bringing distant loci into frequent spatial interaction<sup>65,66</sup>. Of note, *Trim28* deficiency greatly affected the binding of cohesin (SMC1) to chromatin. The binding of SMC1 in the anchor regions of these lost loops were significantly decreased. This suggests that TRIM28 may affect the extrusion function of cohesin and thus the formation of loops. The promoters of T cell activation genes with TRIM28 binding could interact with distal sites (> 100 kb), which were mediated by TRIM28, SMC, CTCF, and RNA Pol II. The observation of reduced SMC1 binding in the absence of *Trim28* suggests a general regulatory mechanism that controls the activity of SMC1. TRIM28 may facilitate the binding of cohesin at the CTCF binding sites. However, how TRIM28 affects the extrusion function of cohesin needs to be further explored.

TRIM28 plays a pivotal role in the activation of CD8<sup>+</sup> T cells, primarily by regulating the expression of IL-2. Compared with naive cells, *Il2* was activated by TRIM28, which mediated the formation of a new chromatin loop between the *Il2* promoter and its upstream enhancer in activated CD8<sup>+</sup> T cells. In the absence of *Trim28*, the chromatin loop also disappeared. Moreover, the enhancer sequence, which is conserved between humans and mice, has been reported to regulate the expression of the *Il2* gene in T cells<sup>61</sup>. Additionally, the accessibility of the *Il2* enhancer is conserved across different immune cells (Supplementary Fig. 9f), including mature B cells, ILC2 Th2 Tfh, and NK cells<sup>62</sup>. Our research provides evidence for a new function of this enhancer in gene regulation. A previous study reported defective signaling of CD28

in TRIM28-deficient CD4<sup>+</sup> T cells<sup>67</sup>. However, CD8<sup>+</sup> T cell activation defect associated with *Trim28* deficiency could not be rescued by increasing concentrations of  $\alpha$ CD28 (Supplementary Fig. 9g). Western blot analysis of proximal TcR and CD28 signaling molecules revealed that no significant difference in the phosphorylation of Akt, PI3K, and ERK2 in *Trim28*<sup>-/-</sup> compared to WT CD8<sup>+</sup> T cells (Supplementary Fig. 9h). Quantitative analysis also showed that the total and phosphorylated levels of Akt, PI3K, and ERK2 were comparable between *Trim28*<sup>-/-</sup> and WT CD8<sup>+</sup> T cells (Supplementary Fig. 9i), suggesting that TRIM28 deficiency did not affect the CD28 co-stimulatory signaling in our system.

In summary, we identified TRIM28 as a critical positive regulator of CD8<sup>+</sup> T cell activation, in which TRIM28 serves as an epigenetic activator and directs CD8<sup>+</sup> T cell activation by regulating epigenetic activation and 3D chromatin looping at key activation-associated genes. Our results implicate epigenetic intervention as possible therapeutics in treatment of tumor and infection.

## Methods

### Mice

C57BL/6, CD45.1, and OT-I (TCR specific for E.G7) mice were maintained in-house. *Il2ra*<sup>-/-</sup> mice were kindly provided by Dr. Yan Shi. *Trim28*<sup>fl/fl</sup> mice reported previously<sup>25,68</sup> were crossed with *Cd8a*<sup>Cre</sup> mice<sup>69</sup>, then were bred onto OT-I mice. 6- to 8-week-old, male and female, age and sex-matched mice were used for all experiments. The mice were maintained under specific pathogen-free (SPF) conditions at Tsinghua University. All studies were approved by the Animal Care and Use Committee of Tsinghua University.

### Naive CD8<sup>+</sup> T cell isolation and in vitro culture

naive CD8<sup>+</sup> T cells were purified from spleens and lymph nodes using Dynabeads™ FlowComp™ Mouse CD8 Kit (Invitrogen). CD8<sup>+</sup>CD25<sup>low</sup>CD44<sup>low</sup>CD62<sup>hi</sup> T cells (naive) were sorted from purified CD8<sup>+</sup> T cells on a FACS Aria (BD) flow cytometer. Then FACS sorted naive CD8<sup>+</sup> T cells with purity greater than 99% were activated with the plate-bound anti-CD3 and anti-CD28 for three days with or without IL-2 and anti-IL2. The information of cytokines and antibodies can be found in Supplementary Tables 2 and 4.

### Flow cytometry

For surface staining, FcR was first blocked by anti-CD16/32 (Biolegend). Then cells were suspended in antibody cocktail together with fixable live/dead cell dye (eBioscience) and incubated in dark at 4°C for 30 minutes. For transcription factor staining, the cells were fixed and stained by Transcription Factor Staining Buffer Set (eBioscience) following the manufacturer's instructions. For cytokine staining, the cells were stimulated with PMA (50 ng/mL, Sigma-Aldrich, MO) and ionomycin (500 ng/mL, Sigma-Aldrich, MO) in the presence of Brefeldin A (Golgstop, BD Bioscience) for 5 h prior to staining with antibodies against surface proteins followed by fixation and permeabilization and staining with antibodies against intracellular antigens. After staining, the cells were acquired on an LSRFortessa (BD) flow cytometer, and data analyzed using FlowJo 10.4.

For detection of phosphorylated STAT5, cells were re-suspended in cold PBS and stained with antibodies against surface molecules. Then the cells were fixed with Phosflow Lyse/Fix buffer (BD Bioscience), followed by 90% methanol permeabilization. The cells were stained with antibodies against phosphorylated STAT5 in PBS. For analysis, the cells were acquired on an LSRFortessa (BD) flow cytometer and data were analyzed using FlowJo 10.4.

Antibody information can be found in Supplementary Table 2.

### Tumor inoculation and LCMV virus infection

E.G7 cells expressing OVA257-264 were cultured in RPMI 1640 medium with 10% FBS, penicillin and streptomycin.  $1 \times 10^6$  E.G7 cells were re-

suspended in 100  $\mu$ L PBS and injected subcutaneously (s.c.) into 6–8-week-old mice. Tumor growth was monitored every 2 or 3 days. Tumor volume was calculated by the following formula: tumor volume =  $0.5 \times \text{length} \times \text{width}^2$ . Mice were ethically euthanized using carbon dioxide asphyxiation after 2 or 3 weeks for phenotypic analyses. Mice were infected intraperitoneally (i.p.) with  $2 \times 10^5$  pfu of LCMV Armstrong expressing GP33-41. Mice were ethically euthanized using carbon dioxide asphyxiation after 1 week for phenotypic analyses.

### Isolation of TILs

E.G7 tumors were digested with 1 mg/mL collagenase D supplemented with 10 U/mL DNase I for 30 min at 37 °C prior to centrifugation on a discontinuous Percoll gradient (GE Healthcare). The maximal tumor burden permitted by the ethics committee is no more than 2000 mm<sup>3</sup>. Tumors were harvested for imaging and tumor weight were measured.

### Adoptive transfer

One million FACS-sorted naive WT and *Trim28*<sup>-/-</sup> OT-I cells were separately transferred (i.v.) into CD45.1 recipients one day prior to EG7 tumor inoculation. 0.5 million FACS-sorted naive CD45.1/2 WT and CD45.2 *Trim28*<sup>-/-</sup> OT-I cells were mixed at 1:1 ratio and transferred (i.v.) into CD45.1 recipients one day prior to E.G7 tumor inoculation.

### In vivo IL-2 treatment

IL-2 (S75406; BioLegend) was dissolved in PBS at a final concentration of 100  $\mu$ g/mL. LCMV Armstrong virus infected-*Trim28*<sup>fl/fl</sup>*Cd8a*<sup>Cre</sup> mice and *Trim28*<sup>fl/fl</sup> mice were intraperitoneally injected with or without mL-2 (10  $\mu$ g per mouse) every two days starting from day 1.

### Co-immunoprecipitation and immunoblot analysis

CD8<sup>+</sup> T cells ( $2 \times 10^7$ ) cultured under anti-CD3/28 for 3 days were resuspended in 1 mL lysis buffer (25 mM Tris, pH 7.4 150 mM NaCl, 1 mM EDTA, 1% NP-40, 5% glycerol plus proteinase inhibitors) and incubated on ice for 30 min. Cells were sonicated for 5 cycles, pelleted by centrifugation, and 10  $\mu$ L anti-TRIM28 antibody (CST, catalog 4123) or control IgG antibody (CST, catalog 2729) was added to and incubated with the supernatant at 4 °C overnight. The next day, the immune complex was captured by Dynabeads protein G, washed thoroughly by lysis buffer for four times and eluted by 1 $\times$  SDS sample loading buffer at 95 °C for SDS-PAGE fractionation and immunoblot analysis. The following antibodies were used for immunoblotting: anti-TRIM28 antibody (CST, catalog 4124), anti-CTCF (CST, catalog 3418), Anti-SMCI (Bethyl Laboratories, A300-055A).

### Retrovirus packaging and infection

Plasmid transfection was performed when 293 T cells were 60%~70% confluent in dish. Chloroquine was added to the dish to 100  $\mu$ M 5 minutes before transfection. For each 10 cm dish, 12  $\mu$ g retrovirus vector, 5  $\mu$ g pCL-eco and 93  $\mu$ L 2 M CaCl<sub>2</sub> were mixed in sterile water to reach final volume of 750  $\mu$ L. 750  $\mu$ L 2 $\times$  HBS was added drop by drop while bubbling vigorously with automatic pipette, and then the mixture was added to dish. Medium was changed 6–8 hours post transfection. The supernatant was harvested, which contained virus particle, 2 days post transfection. After 24-hour activation of T cell, some medium was removed from the wells and around 200  $\mu$ L medium was left. 200–300  $\mu$ L virus supernatant was added to each well, then we supplied polybrene to 8  $\mu$ g/mL in the medium and centrifuged the plate at 1800 rpm, 32 °C for 90 minutes. Medium was refreshed immediately after infection. gRNA silencing efficiency was analyzed 24 hours post infection.

### Plasmids

All the primers used for constructing plasmid were listed in the Supplementary Table 3. gRNA for *Ctcf* were synthesized and inserted into

pWKO-sgRNA(BbsI)- GFP retroviral vector to construct gRNA silencing plasmid.

### Real-time qPCR and RNA-seq experiments

Total RNA from CD8<sup>+</sup> T cells was extracted by TRIzol (Invitrogen) according to manufacturer's instruction. For real-time qPCR, the cDNA was synthesized by reverse transcription using M-MLV Reverse Transcriptase (Promega) according to the manufacturer's instructions. Target genes were amplified by 1 $\times$  Hieff qPCR SYBR Green Master Mix (Yeasen). The mRNA expression of indicated genes were normalized to *Actb*. For RNA-seq, total RNA was sent to BGI Genomics for cDNA library preparation and sequencing. Every sample has two replicates. Primers for RT-qPCR can be found in Supplementary Table 3.

### RNA-seq data analysis

1) Raw data processing. Raw sequencing reads were first adapter-trimmed by Trim Galore v0.4.4 with the “-paired” option, and aligned to mm10 reference genome with HISAT2<sup>70</sup> (version 2.2.1) with “-X 600 -rg-id -rg -known-splicesite-infile -novel-splicesite-outfile -p 25 -reorder” options. StringTie<sup>71</sup> (v2.1.4) was used for transcript quantification with GENCODE vM12 annotation and “-e -B -p 10 -G -o” options. “prepDE.py” script was used to extract the read count information directly from the gtf files generated by StringTie with “-i -g -t” options. The reads count per gene was regarded as the gene expression. 2) Differential Genes Analysis. The gene expression matrix was normalized and analyzed by DESeq2<sup>72</sup> as the software recommended. In detail,  $P\text{-adj} \leq 0.05$  and  $FC \geq 2$  were used to differential genes analysis. 3) Gene enrichment analysis. We used the DAVID Bioinformatics Resources 6.7 for pathway enrichment analysis<sup>73</sup>. All mouse genes were used as the background gene list.

### ChIP experiments

ChIP assay was performed using Active Motif's ChIP assay kit (53035) according to manufacturer's instructions with slight modifications<sup>74</sup>. Briefly, a total of  $1 \times 10^7$  cells were harvested and cross-linked with paraformaldehyde. Then cells were lysed and digested with shearing enzyme followed by sonication. Anti-TRIM28 antibody (Active Motif, 61173), Anti-SMCI (Bethyl Laboratories, A300-055A), and Anti-H3k27ac (Active motif, 39133) was added to supernatant followed by Dynabeads Protein A (Life Technologies) pulling down target fragment. The precipitated DNA was then washed, eluted, de-crosslinked and purified for realtime qPCR analysis or sent to BGI Genomics for cDNA library preparation and sequencing. Every sample has two replicates. Primers for ChIP-qPCR can be found in Supplementary Table 3.

### CUT&Tag experiments

The CUT&Tag experiments were performed as previously described<sup>75</sup> (Vazyme TD903 kit) to generate DNA libraries derived from cells. Antibodies against SMCI (Bethyl Laboratories, A300-055A) and CTCF (Cell Signaling Technology, catalog #3418) were used to target specific chromatin regions. Every sample has two replicates.

### ChIP-seq and CUT&Tag data analysis

1) ChIP-seq and CUT&Tag Peak Calling. The ChIP-seq and CUT&Tag reads were mapped to reference genome by using bowtie2 with the “-p 5 -t -q -N 1 -L 25 -X 2000 -no-mixed -no-discordant” options, followed by removing low mapped quality reads, mitochondrial reads, duplications. PCR duplicates were removed using picard MarkDuplicates. Macs2<sup>76</sup> was used for peak calling with the setting of “-f BAM -B -nomodel -keep-dup all”. 2) ChIP-seq and CUT&Tag Differential Peak Analysis. The differential peak was analyzed by R package DiffBind<sup>77</sup> with the  $FDR \leq 0.01$  and  $FC \geq 1.5$ . ChIP seeker was used for peak annotation. DeepTools was used to generate coverage track file (bigWig) which can be visualized in IGV. 3) To generate a profile plot with

deeptools (3.5.6), first use computeMatrix with parameters “-referencePoint center -missingDataAsZero -p 60 -R input.bed -S input.bw -b 5000 -a 5000 -skipZeros -o heatmap.gz” to calculate average signal values across regions. Signal normalization (CPM) is typically applied during input file creation (using bamCoverage). Next, visualize with plotProfile using “-m (matrix file), -perGroup” to plot each group separately, and “-legendLocation” to position the legend. The Y-axis reflects the average signal intensity, depending on the chosen normalization method.

### ATAC-seq experiments

ATAC-seq DNA library was constructed using TruePrep DNA Library Prep Kit V2 for Illumina and TruePrep Index Kit V2 for Illumina. Briefly, 15,000–50,000 sorted cells were resuspended in 35  $\mu$ L lysis buffer (10 mM Tris-HCl, 10 mM NaCl, 3 mM MgCl<sub>2</sub> 0.1% IGEPAL CA-630) and incubated on ice for 10 min with 3 times vortex. DNA fragmentation was conducted by adding 10  $\mu$ L 5X TTBL, 5  $\mu$ L TTE Mix and shaking at 37°C for 30 min. Fragmented DNA was purified using 1.8 X AMPure beads, barcoded with dual indexes and PCR amplified. Size selection and purification of DNA fragments were done using AMPure beads. Size distribution and molarity of the sequencing library were determined by Qubit (Thermo Fisher Scientific). Sequencing was performed using Illumina X-ten by Novogene. Every sample has two replicates.

### ATAC-seq data analysis

1) ATAC-seq Peak Calling. The ATAC-seq reads were mapped to reference genome by using bowtie2 with the “-p 5 -t -q -N 1 -L 25 -X 2000 -no-mixed -no-discordant” options, followed by removing low mapped quality reads, mitochondrial reads, duplications. Macs2<sup>76</sup> was used for peak calling with the setting of “-f BAM -B -nomodel -keep-dup all”. 2) ATAC-seq Differential Peak Analysis. The differential peak was analyzed by R package DiffBind<sup>77</sup> with the FDR  $\leq$  0.01 and FC  $\geq$  1.5. 3) Motif Enrichment for ATAC-seq Peaks. Homer<sup>78</sup> script findMotifsGenome was used to enrich motifs for ATAC-seq peaks with the “mm10 -p 30 -prepare -size -300,100 -len 8,10,12” options. Q-value  $\leq$  0.1 and p-value  $\leq$  0.01 were used as cutoff for significant enrichment.

### 3C assay

The 3C assay is conducted by initially resuspending five million cross-linked cells in lysis buffer and incubating them on ice for 15 minutes. Afterward, the cells are centrifuged at 2500 g for 5 minutes at 4 °C to remove the lysis buffer and supernatant. The pellet is then resuspended in 342  $\mu$ L of 1x NEBuffer 2 and incubated with 38  $\mu$ L of 10% SDS at 65 °C for 10 minutes to facilitate cell lysis. To quench the SDS, 43  $\mu$ L of 10% Triton X-100 is added and the mixture is incubated at 37 °C for 15 minutes. Subsequently, 12  $\mu$ L of 10x NEBuffer 2 and 400 units of MboI enzyme are introduced to digest the chromatin overnight at 37 °C on a rocking platform. On the subsequent day, the MboI enzyme is inactivated by heating at 65 °C for 25 minutes. The DNA is then religated using T4 DNA ligase, incubated at 24°C for 4 hours, and manually agitated intermittently. The chromatin is de-crosslinked by the addition of 30  $\mu$ L of proteinase K and incubated overnight at 65 °C. DNA extraction is performed using a phenol/chloroform mixture. Finally, PCR and Sanger sequencing are utilized to validate the long-range chromatin interactions, with the specific PCR primers detailed in Supplementary Table 3.

### Hi-C experiments

The Hi-C experiment was performed following the in situ Hi-C protocol<sup>3</sup>. Briefly, a total of  $1 \times 10^6$  cells were isolated and cross-linked with 1% formaldehyde for 10 min at room temperature, and next, 2.5 M glycine solution was added at a final concentration of 0.2 M. Then, the cells were collected, flash-frozen in liquid nitrogen and stored at -80 °C. The fixed cells were then lysed on ice-cold Hi-C lysis

buffer for 30 minutes on ice, followed by Mbo I (NEB, R0147) digestion overnight. The next day, treat sample at 62 °C for 10 min to inactivate Mbo I, and then biotin-14-dATP (Life Technologies, 19524-016) was added to label the digested ends. Then, add ligation master mix (NEB, B0202 & M0202) and connect overnight. On the third day, use Covaris LE220 (Covaris) to break the end-ligated DNA fragments to a suitable length, followed by size selection with AMPure XP beads (Beckman Coulter, A63881). Dynabeads MyOne Streptavidin T1 beads (Life Technologies, 65602) pull down the biotin-labeled fragments, and these fragments are the fragments that truly represent chromatin interactions. Finally, the pull down fragment was purified, and the library was constructed using Illumina primers and protocols (Illumina, 2007). Twelve cycles were amplified by PCR. DNA was purified and the library concentration was measured using Qubit<sup>®</sup> 3.0 fluorometer (Invitrogen). The Agilent Bioanalyzer 2100 (Agilent Technologies) analyzed the library fragment distribution and sequenced on the Illumina HiSeq X Ten platform (Illumina Inc.) if both concentration and length distribution are qualified. Every sample has two replicates.

### Hi-C analysis

We performed read mapping and filtering of the Hi-C data following previous methods. All Hi-C sequencing reads were mapped to the mouse reference genome (mm10) using HiC-Pro (v2.11.4)<sup>79</sup>. We used the iterative correction and eigenvector decomposition (ICE) method to normalize raw interaction matrices.

**A/B compartment analysis.** We used ICE-normalized interaction matrices at 40 kb resolution to detect chromatin compartment types by R-package HiTC<sup>80</sup>. Principal Component Analysis (PCA) was performed on the contact matrix to calculate the first eigenvector (PC1), which distinguishes A and B compartments. For differential compartments analysis, each replicate was analyzed individually. Only compartment stats (A or B) consistent across the two replicates were considered reliable and used for subsequent differential analysis. A genomic region is considered to have a significant shift in compartment status if its compartmentalization changes between two conditions (shifting from Compartment A to B or from B to A).

**TAD analysis.** We used ICE-normalized interaction matrices at 40 kb resolution to call TADs by a Perl script matrix2insulation.pl (<https://github.com/blajoie/crane-nature-2015>). Then we converted adjacent TAD boundaries to corresponding TADs, which were filtered through following steps. First, only TADs with a length larger than 200 kb were kept. Second, TADs located in telomeres or centromeres were removed. For differential TAD analysis, each replicate was analyzed individually. Only TAD coordinates consistent across both replicates were considered reliable and used for subsequent differential analysis. We used BEDtools (intersectBed -f 0.80 - r) to identify conserved TADs that have more than 80% overlapping regions between two samples.

**Domain score.** We employ domain scores<sup>16</sup> for the analysis of differential TADs. Given the TADs identified in the domain segmentation, we calculate an intradomain contact score (simplified to domain score). The domain score is the ratio of the number of contacts that occur between regions within the same TAD (intraTAD contacts) over the total number of intrachromosomal contacts for a TAD (intraTAD + interTAD). When comparing domain scores, we calculated the union of TADs from both cell states. To identify TADs that have a differential domain score we used the bioconductor package limma. We perform quantile normalization (using the normalizeQuantiles function in the limma package) on the domain scores. For each TAD an empirical Bayes moderated t-statistic test is performed. Nominal p-values are corrected using the FDR method. TADs with an FDR value  $<$  0.05 and is present in one state is defined as a specific TAD.

**Loop analysis.** We detected significantly enriched contact interactions using Hi-C computational Unbiased Peak Search (HiCCUPS) (V1.11.04)<sup>31</sup> with default settings (-ignore\_sparsity -m 1024 -r 5000) as described in the previous study<sup>3</sup>. In brief, fold change values quantifying enrichment of contact frequency compared to local background were calculated. To maximize the count of reads for loop analysis, replicates were merged for each sample. Therefore, differential analysis for loops was performed on merged data. Then we tested if the number of the observed contacts is significantly enriched using the Poisson test. P value was Benjamini-Hochberg adjusted to correct for multiple tests. Pixels with enrichment in all local neighborhoods (donut, horizontal, vertical and lower right) were kept. Then cluster of nearby enriched pixels were analyzed using a greedy algorithm. We detected loops at 5 kb resolution. We perform APA on 5 kb resolution contact matrices. To measure the aggregate enrichment of a set of putative peaks in a contact matrix, we plotted the average of a series of submatrices derived from that contact matrix. Each of these submatrices was a 100 kb x 100 kb square centered at a single putative peak in the upper triangle of the contact matrix. The resulting APA plot displayed the total number of contacts that lied within the entire putative peak set at the center of the matrix. Loop set enrichment analysis (LSEA) was modified from PSEA<sup>39</sup> using log<sub>10</sub> (fdrBL) as loop interaction strength. We substitute the interaction strength of loops for the intensity of peaks, while keeping the rest of the analysis pipeline the same.

**MDS analysis.** Multidimensional Scaling (MDS) was employed to analyze the consistency of sample repetitions. MDS is a graphical technique for representing the similarities or differences among items in a low-dimensional space. We utilized the “isoMDS” function from the “MASS” package in R, setting the parameter “metric = TRUE” to ensure the analysis was based on Euclidean distances and used the “stress” measure to assess the fit of the configuration. Additionally, we employed the “ggplot2” package to visualize the MDS results.

### Statistics & reproducibility

Sample sizes were chosen based on previous studies and experimental considerations, without the use of statistical methods to predetermine sample size. No data were excluded from the analyses. Statistical analysis was performed with Graph Prism 8.2.0 (GraphPad software) and presented as mean ± SD unless specifically indicated. For two group comparisons, statistical analysis was performed with unpaired or paired two-tailed Student's t tests. p values less than 0.05 were considered statistically significant.

Proportions' test: the proportion of TRIM28 binding sites in Loops<sup>Activated</sup> (or Loops<sup>naive</sup>) and the proportion of TRIM28 binding sites in all chromatin loops (union of naive and activated CD8<sup>+</sup> T cells) were compared to generate this P-value.

Statistical details for each experiment can be found in the figures and the legends.

### Reporting summary

Further information on research design is available in the Nature Portfolio Reporting Summary linked to this article.

### Data availability

Data associated with all figures and tables is provided in the Source data file and Supplementary files. The raw data generated in this study have been deposited in the the Gene Expression Omnibus (GEO) database [<https://www.ncbi.nlm.nih.gov/geo/>] under the following accession numbers: RNA-seq data (<https://www.ncbi.nlm.nih.gov/geo/query/acc.cgi?acc=GSE260940>), ChIP-seq data (<https://www.ncbi.nlm.nih.gov/geo/query/acc.cgi?acc=GSE260961>), ATAC-seq data (<https://www.ncbi.nlm.nih.gov/geo/query/acc.cgi?acc=GSE260962>), Hi-C data (<https://www.ncbi.nlm.nih.gov/geo/query/acc.cgi?acc=GSE268370>),

and CUT&Tag data (<https://www.ncbi.nlm.nih.gov/geo/query/acc.cgi?acc=GSE277732> and <https://www.ncbi.nlm.nih.gov/geo/query/acc.cgi?acc=GSE269223>). Source data are provided with this paper.

### Code availability

All essential codes used for analysis are available at GitHub (<https://github.com/Ruifengpku/TRIM28>).

### References

- Lieberman-Aiden, E. et al. Comprehensive mapping of long-range interactions reveals folding principles of the human genome. *Science* **326**, 289–293 (2009).
- Dixon, J. R. et al. Topological domains in mammalian genomes identified by analysis of chromatin interactions. *Nature* **485**, 376–380 (2012).
- Rao, S. S. et al. A 3D map of the human genome at kilobase resolution reveals principles of chromatin looping. *Cell* **159**, 1665–1680 (2014).
- Ong, C. T. & Corces, V. G. CTCF: an architectural protein bridging genome topology and function. *Nat. Rev. Genet* **15**, 234–246 (2014).
- Rao, S. S. P. et al. Cohesin loss eliminates all loop domains. *Cell* **171**, 305–320.e324 (2017).
- Davidson, I. F. & Peters, J. M. Genome folding through loop extrusion by SMC complexes. *Nat. Rev. Mol. Cell Biol.* **22**, 445–464 (2021).
- Stik, G. et al. CTCF is dispensable for immune cell transdifferentiation but facilitates an acute inflammatory response. *Nat. Genet.* **52**, 655–661 (2020).
- Kloetgen, A. et al. Three-dimensional chromatin landscapes in T cell acute lymphoblastic leukemia. *Nat. Genet.* **52**, 388–400 (2020).
- Yoshida, H. et al. The cis-regulatory atlas of the mouse immune system. *Cell* **176**, 897–912.e820 (2019).
- Flavahan, W. A. et al. Insulator dysfunction and oncogene activation in IDH mutant gliomas. *Nature* **529**, 110–114 (2016).
- Li, T. et al. Integrative Analysis of Genome, 3D Genome, and Transcriptome Alterations of Clinical Lung Cancer Samples. *Genomics Proteom. Bioinforma.* **19**, 741–753 (2021).
- Xu, J. et al. Subtype-specific 3D genome alteration in acute myeloid leukaemia. *Nature* **611**, 387–398 (2022).
- Du, Z. et al. Allelic reprogramming of 3D chromatin architecture during early mammalian development. *Nature* **547**, 232–235 (2017).
- Lupianez, D. G. et al. Disruptions of topological chromatin domains cause pathogenic rewiring of gene-enhancer interactions. *Cell* **161**, 1012–1025 (2015).
- Ramirez, R. N., Chowdhary, K., Leon, J., Mathis, D. & Benoist, C. FoxP3 associates with enhancer-promoter loops to regulate Treg-specific gene expression. *Sci. Immunol.* **7**, eabj9836 (2022).
- Krijger, P. H. et al. Cell-of-origin-specific 3d genome structure acquired during somatic cell reprogramming. *cell stem cell* **18**, 597–610 (2016).
- Hnisz, D. et al. Activation of proto-oncogenes by disruption of chromosome neighborhoods. *Science* **351**, 1454–1458 (2016).
- Boyman, O. & Sprent, J. The role of interleukin-2 during homeostasis and activation of the immune system. *Nat. Rev. Immunol.* **12**, 180–190 (2012).
- Henning, A. N., Roychoudhuri, R. & Restifo, N. P. Epigenetic control of CD8(+) T cell differentiation. *Nat. Rev. Immunol.* **18**, 340–356 (2018).
- Scharer, C. D., Barwick, B. G., Youngblood, B. A., Ahmed, R. & Boss, J. M. Global DNA methylation remodeling accompanies CD8 T cell effector function. *J. Immunol.* **191**, 3419–3429 (2013).
- Scott-Brown, J. P. et al. Dynamic changes in chromatin accessibility occur in CD8(+) T Cells responding to viral infection. *Immunity* **45**, 1327–1340 (2016).

22. Ozato, K., Shin, D. M., Chang, T. H. & Morse, H. C. 3rd. TRIM family proteins and their emerging roles in innate immunity. *Nat. Rev. Immunol.* **8**, 849–860 (2008).
23. Hatakeyama, S. TRIM family proteins: roles in autophagy, immunity, AND CARCINOGENESIS. *Trends Biochem Sci.* **42**, 297–311 (2017).
24. Tanaka, S. et al. Trim33 mediates the proinflammatory function of Th17 cells. *J. Exp. Med.* **215**, 1853–1868 (2018).
25. Jiang, Y. et al. Epigenetic activation during T helper 17 cell differentiation is mediated by Tripartite motif containing 28. *Nat. Commun.* **9**, 1424 (2018).
26. Seki, T., Yokoyama, Y., Nagasaki, H., Kokuryo, T. & Nagino, M. Adipose tissue-derived mesenchymal stem cell transplantation promotes hepatic regeneration after hepatic ischemia-reperfusion and subsequent hepatectomy in rats. *J. Surg. Res.* **178**, 63–70 (2012).
27. Strelau, M. et al. The cytoplasmic body component TRIM5alpha restricts HIV-1 infection in Old World monkeys. *Nature* **427**, 848–853 (2004).
28. Poole, E. et al. Identification of TRIM23 as a cofactor involved in the regulation of NF-kappaB by human cytomegalovirus. *J. Virol.* **83**, 3581–3590 (2009).
29. Beckstead, R. et al. Bonus, a Drosophila homolog of TIF1 proteins, interacts with nuclear receptors and can inhibit betaFTZ-F1-dependent transcription. *Mol. Cell* **7**, 753–765 (2001).
30. Agarwal, N. et al. TRIM28 is a transcriptional activator of the mutant TERT promoter in human bladder cancer. *Proc. Natl Acad. Sci. USA* **118**, <https://doi.org/10.1073/pnas.2102423118> (2021).
31. Ferri, F., Petit, V., Barroca, V. & Romeo, P. H. Interplay between FACT subunit SPT16 and TRIM33 can remodel chromatin at macrophage distal regulatory elements. *Epigenetics Chromatin* **12**, 46 (2019).
32. Bunch, H. & Calderwood, S. K. TRIM28 as a novel transcriptional elongation factor. *BMC Mol. Biol.* **16**, 14 (2015).
33. Yang, T. et al. HiCRep: assessing the reproducibility of Hi-C data using a stratum-adjusted correlation coefficient. *Genome Res* **27**, 1939–1949 (2017).
34. Meng, X. et al. FBXO38 mediates PD-1 ubiquitination and regulates anti-tumour immunity of T cells. *Nature* **564**, 130–135 (2018).
35. Chikuma, S., Suita, N., Okazaki, I. M., Shibayama, S. & Honjo, T. TRIM28 prevents autoinflammatory T cell development in vivo. *Nat. Immunol.* **13**, 596–603 (2012).
36. Intlekofer, A. M. et al. Effector and memory CD8+ T cell fate coupled by T-bet and eomesodermin. *Nat. Immunol.* **6**, 1236–1244 (2005).
37. Nolz, J. C., Starbeck-Miller, G. R. & Harty, J. T. Naive, effector and memory CD8 T-cell trafficking: parallels and distinctions. *Immunotherapy* **3**, 1223–1233 (2011).
38. Intlekofer, A. M. et al. Anomalous type 17 response to viral infection by CD8+ T cells lacking T-bet and eomesodermin. *Science* **321**, 408–411 (2008).
39. Khan, O. et al. TOX transcriptionally and epigenetically programs CD8(+) T cell exhaustion. *Nature* **571**, 211–218 (2019).
40. Cox, M. A., Kahan, S. M. & Zajac, A. J. Anti-viral CD8 T cells and the cytokines that they love. *Virology* **435**, 157–169 (2013).
41. Liu, Y. et al. IL-2 regulates tumor-reactive CD8(+) T cell exhaustion by activating the aryl hydrocarbon receptor. *Nat. Immunol.* **22**, 358–369 (2021).
42. Schultz, D. C., Friedman, J. R. & Rauscher, F. J. 3rd. Targeting histone deacetylase complexes via KRAB-zinc finger proteins: the PHD and bromodomains of KAP-1 form a cooperative unit that recruits a novel isoform of the Mi-2alpha subunit of NuRD. *Genes Dev.* **15**, 428–443 (2001).
43. Schultz, D. C., Ayyanathan, K., Negorev, D., Maul, G. G. & Rauscher, F. J. 3rd. SETDB1: a novel KAP-1-associated histone H3 lysine 9-specific methyltransferase that contributes to HP1-mediated silencing of euchromatic genes by KRAB zinc-finger proteins. *Genes Dev.* **16**, 919–932 (2002).
44. He, B. et al. CD8(+) T cells utilize highly dynamic enhancer repertoires and regulatory circuitry in response to infections. *Immunity* **45**, 1341–1354 (2016).
45. Pace, L. et al. The epigenetic control of stemness in CD8(+) T cell fate commitment. *Science* **359**, 177–186 (2018).
46. Tang, Z. et al. CTCF-mediated human 3D genome architecture reveals chromatin topology for transcription. *Cell* **163**, 1611–1627 (2015).
47. Chou, C. et al. c-Myc-induced transcription factor AP4 is required for host protection mediated by CD8+ T cells. *Nat. Immunol.* **15**, 884–893 (2014).
48. Kurachi, M. et al. The transcription factor BATF operates as an essential differentiation checkpoint in early effector CD8+ T cells. *Nat. Immunol.* **15**, 373–383 (2014).
49. Tsao, H. W. et al. Batf-mediated epigenetic control of effector CD8(+) T cell differentiation. *Sci. Immunol.* **7**, eabi4919 (2022).
50. Nagasaka, K. et al. Cohesin mediates DNA loop extrusion and sister chromatid cohesion by distinct mechanisms. *Mol. Cell* **83**, 3049–3063.e3046 (2023).
51. Kim, E., Barth, R. & Dekker, C. Looping the genome with SMC complexes. *Annu Rev. Biochem.* **92**, 15–41 (2023).
52. Bauer, B. W. et al. Cohesin mediates DNA loop extrusion by a “swing and clamp” mechanism. *Cell* **184**, 5448–5464.e5422 (2021).
53. Shan, Q. et al. Tcf1-CTCF cooperativity shapes genomic architecture to promote CD8(+) T cell homeostasis. *Nat. Immunol.* **23**, 1222–1235 (2022).
54. Tanaka, S. et al. KAP1 regulates regulatory T cell function and proliferation in both Foxp3-dependent and -independent manners. *Cell Rep.* **23**, 796–807 (2018).
55. Siddiqui, I. et al. Intratumoral Tcf1(+)PD-1(+)/CD8(+) T cells with stem-like properties promote tumor control in response to vaccination and checkpoint blockade immunotherapy. *Immunity* **50**, 195–211.e110 (2019).
56. Miller, B. C. et al. Subsets of exhausted CD8(+) T cells differentially mediate tumor control and respond to checkpoint blockade. *Nat. Immunol.* **20**, 326–336 (2019).
57. Cai, X. et al. Tripartite motif containing protein 27 negatively regulates CD4 T cells by ubiquitinating and inhibiting the class II PI3K-C2beta. *Proc. Natl Acad. Sci. USA* **108**, 20072–20077 (2011).
58. Bruzzaniti, S. et al. CD4(+) T cell defects in a mulibrey patient with specific TRIM37 mutations. *Front Immunol.* **11**, 1742 (2020).
59. Ryan, R. F. et al. KAP-1 corepressor protein interacts and colocalizes with heterochromatic and euchromatic HP1 proteins: a potential role for Kruppel-associated box-zinc finger proteins in heterochromatin-mediated gene silencing. *Mol. Cell Biol.* **19**, 4366–4378 (1999).
60. Cheng, C. T., Kuo, C. Y. & Ann, D. K. KAP1 in charge of multiple missions: Emerging roles of KAP1. *World J. Biol. Chem.* **5**, 308–320 (2014).
61. Kizer, K. O. et al. A novel domain in Set2 mediates RNA polymerase II interaction and couples histone H3 K36 methylation with transcript elongation. *Mol. Cell Biol.* **25**, 3305–3316 (2005).
62. Guenther, M. G., Levine, S. S., Boyer, L. A., Jaenisch, R. & Young, R. A. A chromatin landmark and transcription initiation at most promoters in human cells. *Cell* **130**, 77–88 (2007).
63. Yang, Y. et al. HIF-1 Interacts with TRIM28 and DNA-PK to release paused RNA polymerase II and activate target gene transcription in response to hypoxia. *Nat. Commun.* **13**, 316 (2022).
64. Nora, E. P. et al. Spatial partitioning of the regulatory landscape of the X-inactivation centre. *Nature* **485**, 381–385 (2012).
65. Fudenberg, G. et al. Formation of chromosomal domains by loop extrusion. *Cell Rep.* **15**, 2038–2049 (2016).
66. Sanborn, A. L. et al. Chromatin extrusion explains key features of loop and domain formation in wild-type and engineered genomes. *Proc. Natl Acad. Sci. USA* **112**, E6456–E6465 (2015).

67. Gehrman, U. et al. Critical role for TRIM28 and HP1beta/gamma in the epigenetic control of T cell metabolic reprogramming and effector differentiation. *Proc. Natl Acad. Sci. USA* **116**, 25839–25849 (2019).
68. Zhou, X. F. et al. TRIM28 mediates chromatin modifications at the TCRalpha enhancer and regulates the development of T and natural killer T cells. *Proc. Natl Acad. Sci. USA* **109**, 20083–20088 (2012).
69. Maekawa, Y. et al. Notch2 integrates signaling by the transcription factors RBP-J and CREB1 to promote T cell cytotoxicity. *Nat. Immunol.* **9**, 1140–1147 (2008).
70. Kim, D., Paggi, J. M., Park, C., Bennett, C. & Salzberg, S. L. Graph-based genome alignment and genotyping with HISAT2 and HISAT-genotype. *Nat. Biotechnol.* **37**, 907–915 (2019).
71. Pertea, M. et al. StringTie enables improved reconstruction of a transcriptome from RNA-seq reads. *Nat. Biotechnol.* **33**, 290–295 (2015).
72. Love, M. I., Huber, W. & Anders, S. Moderated estimation of fold change and dispersion for RNA-seq data with DESeq2. *Genome Biol.* **15**, 550 (2014).
73. Jiao, X. et al. DAVID-WS: a stateful web service to facilitate gene/protein list analysis. *Bioinformatics* **28**, 1805–1806 (2012).
74. Wang, X. et al. Febrile temperature critically controls the differentiation and pathogenicity of t helper 17 cells. *Immunity* **52**, 328–341.e325 (2020).
75. Kaya-Okur, H. S. et al. CUT&Tag for efficient epigenomic profiling of small samples and single cells. *Nat. Commun.* **10**, 1930 (2019).
76. Zhang, Y. et al. Model-based analysis of ChIP-Seq (MACS). *Genome Biol.* **9**, R137 (2008).
77. Ross-Innes, C. S. et al. Differential oestrogen receptor binding is associated with clinical outcome in breast cancer. *Nature* **481**, 389–393 (2012).
78. Heinz, S. et al. Simple combinations of lineage-determining transcription factors prime cis-regulatory elements required for macrophage and B cell identities. *Mol. Cell* **38**, 576–589 (2010).
79. Servant, N. et al. HiC-Pro: an optimized and flexible pipeline for Hi-C data processing. *Genome Biol.* **16**, 259 (2015).
80. Servant, N. et al. HiTC: exploration of high-throughput ‘C’ experiments. *Bioinformatics* **28**, 2843–2844 (2012).
81. Durand, N. C. et al. Juicer provides a one-click system for analyzing loop-resolution hi-c experiments. *Cell Syst.* **3**, 95–98 (2016).

## Acknowledgements

We thank Dr. Yan Shi for providing *Il2ra*<sup>-/-</sup> mice and Dr. Wenwen Zeng for providing LCMV Armstrong virus. This work was supported by grants from Natural Science Foundation of China (31991173 and 31991170), National Key Research and Development Program of China (2021YFC2302403), CAMS Innovation Fund for Medical Sciences (2022-I2M-5-01), and Boehringer Ingelheim.

## Author contributions

K.W., R.F.L., and C.D. designed the project and analyzed the data. K.W. and R.F.L. conducted the experiments. T.X., Q.L.S., Y.Z.C., P.W., W.X., X.Y.G., Z.X.Z., and H.F. helped with the experiments. R.F.L. and X.H.Z. analyzed the bioinformatics data. K.W., R.F.L., C.D., L.N., and B.W.X. prepared the manuscript.

## Competing interests

The authors declare no competing interests.

## Additional information

**Supplementary information** The online version contains supplementary material available at <https://doi.org/10.1038/s41467-025-56029-z>.

**Correspondence** and requests for materials should be addressed to Chen Dong.

**Peer review information** *Nature Communications* thanks Ferhat Ay, Charalampos Spilianakis and Wei Zhao for their contribution to the peer review of this work. A peer review file is available.

**Reprints and permissions information** is available at <http://www.nature.com/reprints>

**Publisher's note** Springer Nature remains neutral with regard to jurisdictional claims in published maps and institutional affiliations.

**Open Access** This article is licensed under a Creative Commons Attribution-NonCommercial-NoDerivatives 4.0 International License, which permits any non-commercial use, sharing, distribution and reproduction in any medium or format, as long as you give appropriate credit to the original author(s) and the source, provide a link to the Creative Commons licence, and indicate if you modified the licensed material. You do not have permission under this licence to share adapted material derived from this article or parts of it. The images or other third party material in this article are included in the article's Creative Commons licence, unless indicated otherwise in a credit line to the material. If material is not included in the article's Creative Commons licence and your intended use is not permitted by statutory regulation or exceeds the permitted use, you will need to obtain permission directly from the copyright holder. To view a copy of this licence, visit <http://creativecommons.org/licenses/by-nc-nd/4.0/>.

© The Author(s) 2025